

UNIVERSITÀ DEGLI STUDI DELLA CALABRIA

Dipartimento di Fisica

Tesi di Dottorato di Ricerca
in Fisica

PERIODIC AND APERIODIC
STRUCTURES REALIZED BY
INNOVATIVE SOFT-MATTER BASED
TECHNIQUES

Melissa Infusino



Supervisore

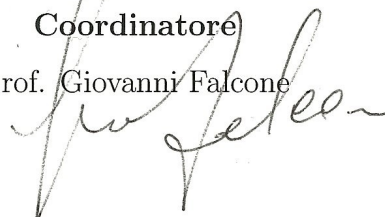
Prof. Cesare Umeton,

Prof. Raffaele Agostino



Coordinatore

Prof. Giovanni Falcone



Dicembre 2010

DOTTORATO DI RICERCA XXIII Ciclo
Settore Scientifico Disciplinare (SSD) FIS/03

Contents

Abstract	3
Introduction	4
Motivation and Objectives	4
1 HPDLC/POLICRYPS structures	9
1.1 Nematic Liquid Crystals	9
1.1.1 The effect of a static electric field	11
1.1.2 Birefringence	12
1.2 Polymers and Photo-Polymerization	14
1.3 Polymer Dispersed Liquid Crystal	17
1.4 Holographic Gratings	19
1.5 Thick and Thin Gratings	21
1.5.1 Holographic Polymer Dispersed Liquid Crystals	23
1.6 POLICRYPS Gratings	24
1.6.1 A model for POLICRYPS and HPDLC formation	28
1.7 SLM Technology	31
2 POLICRYPS visible curing	35
2.0.1 Pre-polymer mixtures tested	36
2.0.2 1D Raman Nath Gratings	41

3	Pattern Generation via computer holography	45
3.1	IFTA implementation an results	47
3.2	Limitations	51
4	Periodic and aperiodic structure realized by direct imaging	56
4.1	From indirect to direct imaging	56
4.1.1	Edge enhancing effect	57
4.2	1D Raman Nath grating	59
5	Periodic and aperiodic structure realized by direct imaging	63
5.1	2D Periodic gratings	63
5.2	Aperiodic structures: fork gratings	67
6	Di-block copolymer confined in thin films	70
6.1	Di-block Copolymer	71
6.2	Thin film lamellæ organization	73
6.3	Samples preparation and characterization	75
6.4	Results for thermal annealing	77
6.5	Solvent annealing results	79
	Conclusions	84
	Bibliography	87

Abstract

Il presente lavoro di tesi è basato sullo studio e l'utilizzo di tecniche sperimentali per la realizzazione di strutture periodiche ed a-periodiche su diverse scale di grandezza. La prima tecnica oggetto di studio rappresenta un nuovo approccio rispetto alle usuali tecniche olografiche e prevede l'utilizzo delle più recenti tecnologie realizzate nell'ambito dell'olografia diffrattiva, quali i modulatori di fase spaziale. I modulatori di fase spaziale consentono la produzione di distribuzioni di intensità sia periodiche che a-periodiche ed in generale rendendo possibili geometrie difficilmente realizzabili con le classiche tecniche di interferenza a multi-fascio. Il sistema fotosensibile di partenza è costituito da una miscela di pre-polimeri e cristalli liquidi nematici: la separazione di fase tra le due componenti è indotta dalla fotopolimerizzazione. L'impiego dei cristalli liquidi consente la realizzazione di strutture dinamiche le cui proprietà ottiche sono modificabili attraverso l'applicazione di stimoli esterni, quali campi elettrici ed ottici. Le strutture realizzate hanno una periodicità micrometrica che le rende applicabili nel campo dell'ottica. La seconda tecnica studiata si basa su fenomeni di auto-assemblaggio nei polimeri a blocchi e consente il raggiungimento di scale di grandezza inferiori: la periodicità delle strutture realizzate raggiunge infatti poche decine di nanometri. Nella tecnica di auto-assemblaggio la separazione di fase tra le componenti è regolata semplicemente dalla temperatura del sistema e le strutture risultanti hanno delle caratteristiche fortemente dipendenti dalle dimensioni dei costituenti.

Introduction

Motivation and Objectives

The present PhD work is based on the realization of soft-matter periodic and a-periodic gratings by using two different experimental techniques. The first structures have been realized and characterized in the Liquid Crystal Laboratories (UNICAL). The chosen technique exploits recent developments in the field of holography and the quality of the realized structures depends both on pattern designing and on materials response to light. The other structures have been realized during a five months stage, in the Centre de Recherche Paul Pascal of Bordeaux, using a self assembling technique involving Diblock copolymers. The properties of the resulting structures depends exclusively on the materials choice and on their interaction with substrates.

▷ **Holographic fabrication of 2D Switchable multi-component structures:**

In this work we are presenting a method developed for the realization of two dimensional switchable photonic structures. The structures realized are an alternation in space of polymer and liquid crystal; the periodicity of the structures and the difference between the refractive index of the two media determine their optical properties. The advantage of using liquids crystal instead of any other material is that its refractive index can be controlled by the application of an external electric field. With a proper choice of the materials, it

is possible to realize structures that have completely switchable optical properties. The technique used for the realization of the structures is well known and it is based on the holographic polymerization of a photosensitive mixture of liquid crystal and monomer. In the past two decades it has been widely exploited for the realization of diffraction gratings [1, 2] known as HPDLC, acronym for Holographic Polymer Dispersed Liquid Crystal. In 2000/2001 a new kind of multi-component gratings have been developed [3, 4], whose acronym is POLICRYPS (POLYmer LIquid CRYstal Polymer Slices). Details of HPDLC and POLICRYPS techniques will be discussed in the next section. The realization of the policryps gratings is characterized by a high diffusive curing, that gives them interesting characteristics. As their name suggest they are composited by continuous and well-aligned nematic films separated by polymer slices. Thus their morphology represents an improvement in comparison with HPDLC gratings, where the liquid crystal is gathered in droplets inside the polymeric matrix. The POLICRYPS technique has been extensively studied and the realized samples present excellent optical performances [5–7]. In literature several examples of two dimensional HPDLC structures realized by multi-beam interference holography [8–10] and more recently with alternative techniques [11, 12] are reported, but till now no one tried to do something similar by using POLICRYPS. Extending the use of the POLICRYPS fabrication technique to the realization of two dimensional periodic and a-periodic structures is not a trivial problem. First of all, the POLICRYPS optical characteristics worth an attempt finalized to the applications. Furthermore the realization of different geometries can be the base for a further understanding of the highly non linear mechanisms involved in the formation of POLICRYPS. The fabrication of a two dimensional light pattern trough interference holography can really become a tricky problem. The complexity of the interference

optical set-up depends on the design of the pattern we want to realize. More the set-up is complicated, more it will be affected by instability problems that can spoil the quality of the holographic recording. Therefore, we have chosen to follow an alternative approach [11, 13] that allow to realize any kind of two dimensional light pattern by using a single laser beam. This approach involves the exploitation of a Spatial Light Modulator (SLM) [14], that is a high resolution display, whose pixels can be separately controlled to apodize an impinging laser beam.

▷ **Diblock copolymer self assembling in thin films**

The aim of the project conducted in the CRPP of Bordeaux is the study and the realization of an anisotropic dielectric template for the organization of plasmonic nano-particles. Diblock copolymers (DBC), because of their self-assembling ability in periodic structures with a very small periodicity (typically 30-40 nm), are very good candidates for this purpose. The natural segregation of DBC can be steered by temperature, but in absence of constrains the size of the ordered domains is micro-metric. The strategy that has been chosen to obtain ordered structures, at a macroscopic scale, is the realization of DBC thin films. The study realized is based principally on the realization of DBC thin films on silicon substrates and on the characterization of their ordered status.

Organization

This thesis is divided into five Chapters. The first four chapters are related to the holographic realization of multi-component gratings. The last chapter, instead, is entirely dedicated to the realization of DBC thin films on given substrates.

In the First Chapter we briefly introduce the characteristics of materials and

of used techniques . We start with the nematic liquid crystals, whose treatment is far from being exhaustive; we focus our attention only on those liquid crystal properties that are important for the realization of electro-optical devices. A section is devoted to photo-polymers, polymer dispersed liquid crystal materials and holographic realization of gratings based on these kind of multi-component systems. A further section is dedicated to the POLICRYPS curing, that is the holographic photo-polymerization technique we used for the realization of our switchable photonic structures. The last section of the first chapter describes the working principle of spatial light modulator and it introduces the problematic related to the use of this instrument.

The second chapter deals with the description of the strategy followed during this work. The first section concerns the study of suitable materials for the visible POLICRYPS curing. This is a work we developed in parallel with the study of the light pattern generation described instead in chapter three. In order to test the materials, 1D Raman-Nath diffraction gratings have been realized by using a simple interferometric set-up. The second section describes the two approaches followed to produce a generic two dimensional light pattern with a SLM. The first approach consist in the use of the SLM as the physical support for a phase hologram. The desired pattern is reconstructed in the focal plane of a lens. The implementation of an Iterative Fourier Transform Algorithm (IFTA) for the calculation of the suitable phase function has been performed. The second approach allowed to obtain the desired pattern, charging on the SLM almost its direct image. In the fourth chapter the morphological and electro-optical properties of the realized structures are presented. The fifth chapter describes the work realized during the stage hosted by the CRPP of Bordeaux. A first section introduces the Diblock copolymer and their behavior when they are confined in thin films. Another section is dedicated to the ex-

perimental techniques used to induce lamellar organization. A further section report the characterization related to the surface morphology of the films. The conclusions and the perspectives for future developments of this PhD work are discussed in a last section.

Chapter 1

HPDLC/POLICRYPS structures

1.1 Nematic Liquid Crystals

“Liquid crystal are materials that, in addition to the solid crystalline and liquid phases, exhibit intermediate phases where they flow like liquids, yet possessing some physical characteristics of crystals. The materials that exhibit these unusual phases are often called mesogens and the various phases in which they could exist mesophases“ [15]. In nature it exists a huge variety of mesogens and of mesophases. It is possible to classify liquid crystals considering the physical parameter that determines the appearance of the mesophase [15, 16]. A classification of the different mesophases also exist and it is essentially based on their symmetry [16]. In this work we dealt uniquely with thermotropic liquid crystals [17] and with their nematic phase. The thermotropic liquid crystal mesophases exist only in a certain temperature range between the melting point (phase transition from solid to liquid crystal) and the clearing point (transition from liquid crystal phase to the isotropic liquid).

They are composed by elongated molecules with a typical length ~ 20 –

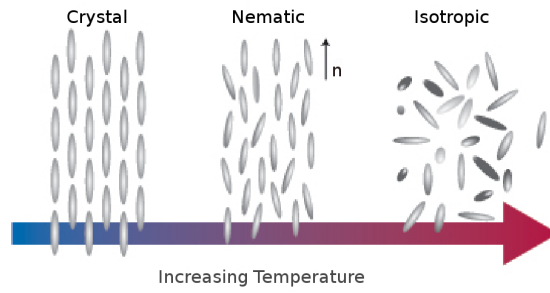


Figure 1.1: The Nematic phase exists only in a certain range of temperatures 40\AA and a typical diameter $\sim 4 - 5\text{\AA}$ [18]. The centers of gravities of the molecules in the nematic phase do not exhibit any long range order but within mesoscopic domains their long axes are aligned in average along a preferential direction, given by the nematic director \mathbf{n} . The complete rotational symmetry around \mathbf{n} make it an uniaxial phase. It has many consequences and two of them are very interesting for applications: firstly the nematic phase is birefringent [19] (the director \mathbf{n} is its optical axis), secondly the dielectric anisotropy of liquid-crystal molecules make them susceptible to electric fields. These are the fundamental properties that enable designing of switchable electro-optical liquid-crystal devices.

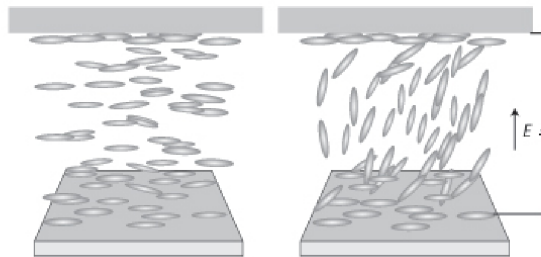


Figure 1.2: Liquid-crystal molecules with a positive dielectric anisotropy will align along the direction of an applied electric field

In order to exploit the anisotropic properties of the nematic phase and

make them effective at a macroscopic scale, it is important to obtain an uniform alignment of the different nematic domains. In an actual sample the orientation of \mathbf{n} is imposed by boundary conditions. If no particular care is taken, boundary conditions will vary over the sample bringing to variations in the director pattern and in the birefringence. This last aspect is responsible for the name nematics that comes from the ancient Greek $\nu\eta\mu\alpha$ and means thread. The discontinuity in the molecular director alignment observed under a microscope between cross polarizers looks exactly like dark and flexible filaments. They has been observed in the early ears of the last century by Granjean and Friedel, while later Frank gave them the name of "disclinations" [20,21].

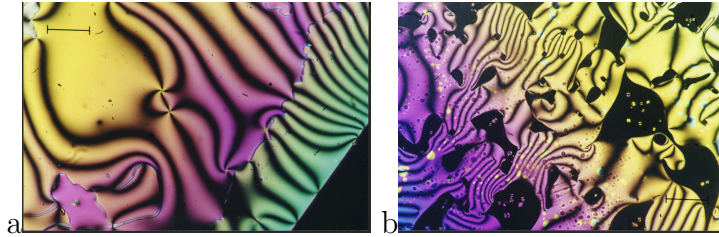


Figure 1.3: Characteristic "threading" observed in nematic textures the dark threads observed through out of the colored regions correspond to molecular domains which are aligned along the direction of one of the optical polarizers. *Pictures by Lee Y.Park*

1.1.1 The effect of a static electric field

NLCs have not an isotropic dielectric response, which depends instead, on the angle that an external electric field forms with the nematic director. Furthermore, only non conductive NLC materials are taken into account, therefore this treatment [22] is based on the hypothesis of perfect insulators. The most generic expression for the dielectric displacement is given by equation 1.1

$$D = \varepsilon_{\perp} E + (\varepsilon_{\parallel} + \varepsilon_{\perp})(\mathbf{n} \cdot E)\mathbf{n} \quad (1.1)$$

where ε_{\perp} (ε_{\parallel}) is the dielectric constant exhibited when the field is perpendicular (parallel) to the director. The difference $\varepsilon_a = \varepsilon_{\parallel} - \varepsilon_{\perp}$ is defined "dielectric anisotropy" and it can be positive or negative, depending on the detailed chemical structure of molecules. If the molecules present an induced dipole moment parallel to their long axes, the dipole can be efficiently oriented by a field parallel to \mathbf{n} . In this case $\varepsilon_a > 0$. If the molecules present an induced dipole moment more or less perpendicular to their long axes, it can be oriented by a field perpendicular to \mathbf{n} and $\varepsilon_a < 0$. The electric contribution to the free energy density is given by equation 1.2.

$$-1 \frac{4}{\pi} \int \mathbf{D} \cdot \mathbf{E} = -\varepsilon_{\perp} \frac{8}{\pi} - \varepsilon_a \frac{8}{\pi} (\mathbf{n} \cdot \mathbf{E})^2 \quad (1.2)$$

The first term is independent of orientation, but the second term induces a parallel alignment if $\varepsilon_a > 0$ and a perpendicular alignment if $\varepsilon_a < 0$. However, the strength of the applied field has to be larger than a certain threshold in order to overcome the elastic forces of the liquid crystal. This threshold is called the Fredericksz threshold and the transition from an undistorted director configuration to a distorted one is called the Fredericksz transition or the Fredericksz effect.

1.1.2 Birefringence

NLCs are uniaxial optical media [19]. The propagation of a light wave in such media can be easily understood considering the index ellipsoid associated to the material. The optical axis in NLCs coincides with the nematic director \mathbf{n} , in fig 1.4 it lays along z.

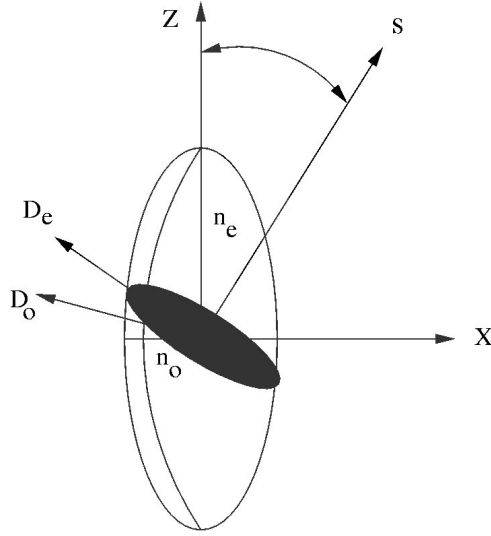


Figure 1.4: Index ellipsoid for an uniaxial medium

The ellipse given by the intersection between the ellipsoid and the plane perpendicular to the direction of propagation \mathbf{s} gives the values of the two refractive indexes for the "ordinary" and the "extraordinary" waves, along with the directions of oscillation of the two field D_e and D_o . A rigorous exposition can be found in [23]. The two waves generated in the anisotropic medium travel with a different speed, $(\frac{c}{n_o}$ and $\frac{c}{n_e}$) and the phase delay between the two waves result in a change in the polarization status of the outgoing light. While the ordinary index has a constant value, n_o ,

$$n_o(\theta) = \text{cost} \quad (1.3)$$

the extraordinary index depends on the angle θ between \mathbf{s} and \mathbf{n} .

$$n(\theta) = \frac{n_e n_o}{\sqrt{n_e^2 \cos^2 \theta + n_o^2 \sin^2 \theta}} \quad (1.4)$$

Thus, if a light beam is propagating perpendicularly to the optical axis and its E-vector is parallel to the optical axis it sees the refractive index n_e . If the E-vector is perpendicular to the optical axis, the wave sees the refractive index

n_o . If, instead, the E-vector makes some angle with the optic axis, the wave is splits up into two waves (ordinary and extraordinary). The optical anisotropy of the medium is called birefringence, and it is measured by expression 1.5

$$\Delta n = n_e - n_o \quad (1.5)$$

In general $n_e > n_o$; Δn is therefore positive and it varies from values close to zero to about 0.4.

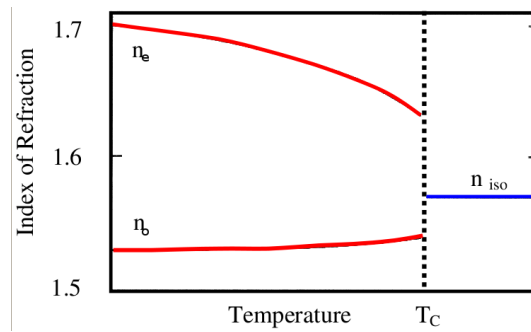


Figure 1.5: Extraordinary and Ordinary Refractive Index vs Temperature

The NLCs birefringence is a physical property that depends on the degree of orientational order of molecules, therefore, it is a function of temperature.

In Figure 1.5 the indexes of refraction are plotted as functions of temperature: The optical anisotropy Δn decreases as temperature increases and vanishes at a certain value, which corresponds to the Nematic-Isotropic transition temperature of the material.

1.2 Polymers and Photo-Polymerization

Polymers are macromolecules composed by the repetition of the same building blocks called monomers, linked each other by covalent bonds. Depending on

monomer functionality ¹, different molecular architectures can be obtained. The simplest one is the linear chain (fig.1.6a), and it occurs with bifunctional monomers. In this case, polymers chains are linked by weak bonds such as van der Waals, polar or hydrogen bonds. A branched polymer (fig.1.6b) is a molecule composed of a main chain with one or more side chains or branches; for their formation higher functionality monomers are required. In crosslinked polymers (fig.1.6c-d), adjacent linear chains are joined one to another trough strong covalent bonds, resulting in a three-dimensional network.

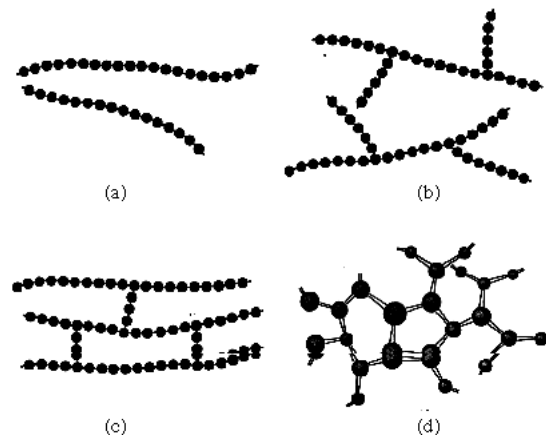


Figure 1.6: a)Linear-chain polymer b)Branched-chain polymer c)Network or gel polymer

There are different processes for the polymer chains formation, but they can be classified in three fundamental types: The chain-growth polymerization, the condensation polymerization and the step-growth polymerization [24].

- The chain-growth polymerization consist in the sequential addition of one bifunctional or polyfunctional monomer to a growing polymer chain P_n without the elimination of any part of the monomer molecule. With the subscript n representing the chain length, the polymerization can be

¹the monomer functionality is related to the number of double bonds that can react in the polymerization process

schematically represented as follows:



where M represents a monomer molecule. This chain growth step is usually very fast.

- In the condensation process, polymers are formed from bifunctional or polyfunctional monomers with the elimination of small molecular species. This reaction can occur between any two growing polymer molecules and can be represented by



where P_m and P_n are polymer chains and W is the condensation product.

- Step-growth polymerization has a mechanism similar to the one exhibited by condensation polymerization but includes reactions like the one in (1.7), where no molecular species are eliminated.

In chain-growth polymerization, it is found that individual molecules start growing and grow rapidly to form long chain molecules. In step-growth polymerization, on the other hand, the monomer molecules react with each other at the beginning to form low-molecular-weight polymers. These low-molecular-weight molecules continue to react with each other to form continually growing chains. Thus, formation of long chains molecules in this case is much slower. In order to trigger the process, an external stimulus is necessary. It can be heat, gamma radiation or light. The present work deals uniquely with free-radical photo-polymerization processes. Light-induced polymerization has several advantages over other methods. The process can be controlled by selecting different irradiation wavelength and light intensity. Moreover, light can be focused on a particular site, thus, polymer can be formed where it is desired [25].

To make the pre-polymer mixture sensible to a particular light wavelength, a small amount of photoinitiator molecules is added. There are two types of photo-initiators: the cleavable photoinitiators and the photo-initiators involving electron-transfer reactions. In the first case the absorption of a (UV or visible) photon $h\nu$ brings to the homolytic cleavage of a bond in the photoinitiator molecule, yielding free radicals. (fig 1.7) In the second case, the photoinitiator in the excited state interacts with a second molecule (a co-initiator) to generate free radicals [26]. The presence of an unpaired electron in radicals makes them able to attack the double bonds present in monomers. The radical activation of a monomer gives the start to the process, whose evolution depends on the particular pre-polymer, as already explained.

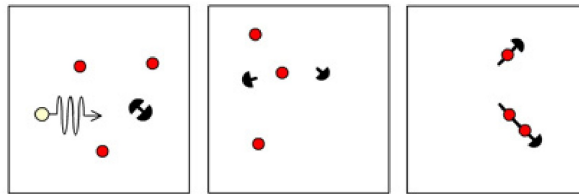


Figure 1.7: Photo-polymerization initiation

1.3 Polymer Dispersed Liquid Crystal

Among the most investigated liquid crystalline composite materials there are Polymer-Dispersed Liquid Crystals (PDLCs). Since the late 80s, PDLCs have attracted a wide interest, both from the scientific community, for the aspects of related basic researches, and from industries, due to the relevance of these systems for display and window technology [27]. In a PDLC material, liquid crystal droplets are randomly distributed within a rigid polymer matrix. The droplet size can be controlled during the phase separation process and diameter can vary from $0.01\mu\text{m}$ to $20\mu\text{m}$. The initial polymer-liquid crystal blend

is characterized by a low molecular weight for the liquid crystal (below 40%). Three different methods can be used for the PDLCs formation [18, 28]. They can be divided into two classes: phase separation methods [29] and encapsulation methods [30]. The first is the so called 'Polymerization induced phase separation' (PIPS). The polymerization process can be induced thermally or by UV or visible light [31]. In the last case the curing intensity can be used as a control parameter of the droplet size. Furthermore, other factors like concentrations of the species, viscosity of the polymer, solubility of liquid crystal and diffusion rates have to be taken into account. The second method is the so called "Thermal Induced Phase separation" (TIPS). It is used with thermoplastic polymers that melt below their decomposition temperature. The system of a liquid crystal dispersed in the melted polymer is cooled down bringing to phase separation. The cooling rate plays an important role in the determination of the droplet size. The third method is the Solvent Induced Phase separation (SIPS). The liquid crystal and the polymer are dissolved in a common solvent. The evaporation of the solvent brings to the phase separation. The evaporation rate determines the droplet size.

The alignment of the liquid crystal inside droplets, in the absence of an external alignment field, depends on the liquid crystal-polymer interaction at the boundary. In case of a tangential anchoring to the polymer surrounding walls, a bipolar configuration is the most stable for the NLC director.

This configuration is characterized by two singular points at the opposite poles (1.8 b). In case of a normal anchoring it is possible to have a star configuration with a singular point in the middle of the sphere (1.8 a). PDLC based devices exploit the possibility of an external control on the optical transmission, obtained by inhibiting or enhancing light scattering. To enhance scattering the droplet size is chosen comparable with the wavelengths of the impinging light.

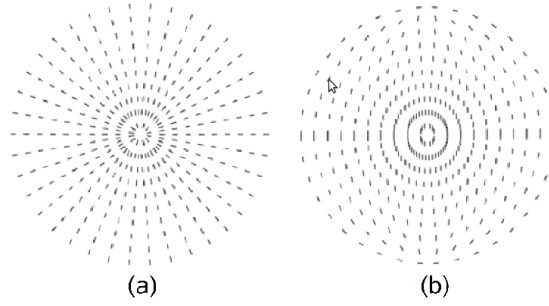


Figure 1.8: a)radial configuration b) biaxial configuration

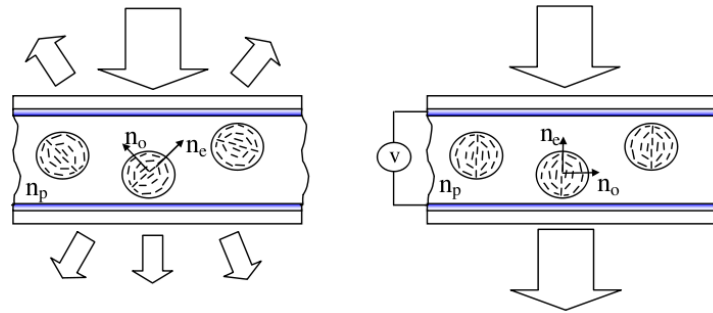


Figure 1.9: The scheme illustrates the operating mode of a pdlc sample

The orientation of the droplet axes is random and, as a consequence, the index mismatch changes from droplets to the polymer binder, causes a strong scattering. Upon the application of an electric field, droplets will be aligned and the system will become clear as the refractive index of the liquid crystal droplet matches the one of the isotropic polymer background.(fig 1.9)

1.4 Holographic Gratings

Holography is the process of recording the complete information of the optical electric field in both amplitude and phase; consequently a real three-dimensional image can be reconstructed [32, 33]. Since most of recording materials are sensitive only to the intensity of light, interference is a very convenient way to convert a phase information into an amplitude information.

In the holographic reconstruction of a three dimensional object, the hologram is formed by the interference of the light diffracted by the object with a reference beam. In a second step the recorded information can be read back by a reconstructing light beam [34]. Photopolymers are holographic materials that have been widely used in the fabrication of Holographic optical elements; diffraction gratings can be obtained by holographic interference patterning and subsequent modulation of the refractive index in photopolymer materials. The recording of a holographic grating can be considered as a simpler special case, where both reference and object beam are two coherent plane waves. In this case, the interference produces a sinusoidal intensity pattern whose periodicity, in the transmission mode case², is given by the following expression:

$$\Lambda = \frac{\lambda_w}{2n_0 \sin\theta_w} \quad (1.8)$$

Where λ_w is the wavelength of the writing laser beam, n_0 is the refractive index of the medium, θ_w is half times the angle between the two writing beams.

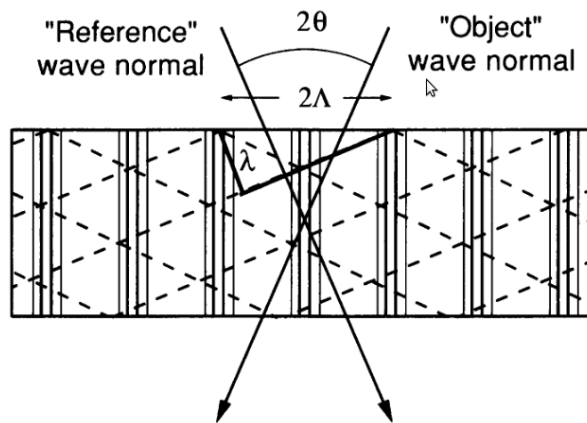


Figure 1.10: holographic recording in a photosensitive material

The diffractive properties of a grating represent its main characteristics. In fact a grating is a periodic dielectric structure able to modulate the phase or the

²Holographic gratings are divided in reflection and transmission mode gratings [35].

amplitude of an incident light. Due to this periodic modulation, the impinging light is split into different beams traveling along separated directions, which depend on the grating spacing and on the light wavelength; therefore a grating acts as a dispersive optical element. The diffraction skill is measured by the diffraction efficiency η , defined, in general, as the ratio between the intensity of the selected diffracted beam and the intensity of the incident beam.

1.5 Thick and Thin Gratings

Diffraction gratings behave differently depending on the relation between their periodicity and their thickness; it is therefore common use to categorize gratings as thick or thin depending on this relation. The occurrence of the two diffraction regimes may be determined using a number of different criteria [36]. In general the distinctions is made by considering a dimensionless Klein-Cook parameter Q [37]:

$$Q = \frac{2\pi d\lambda}{n_0\Lambda^2} \quad (1.9)$$

where d is the thickness of the grating, Λ is the grating period, n_0 is the spatially averaged refractive index of the medium, λ is the incident wavelength.

When $Q > 10$ a grating is said to be thick (or a volume grating) and it corresponds to the Bragg regime. In this case, the equation for the maxima position is the well known Bragg law, that comes from the constructive interference condition for waves diffracted by two adjacent planes. Maxima occur when:

$$N\lambda = 2n_0\Lambda\sin\theta \quad (1.10)$$

where N is an integer, n_0 is the averaged refractive index of the medium, θ is the incidence angle. The angle that hold the relation for $N = \pm 1$ is

called Bragg angle, and it is indicated with θ_B . However when the incident angle slightly deviates from θ_B , relatively weak diffraction can also be observed, even if in general these gratings are strongly selective in angle of incidence. Such structures exhibit only two diffraction orders (zeroth- and first-order): this means that the energy is not dispersed, but it can be concentrated almost totally into the first diffracted order. The diffraction efficiency of the transmission volume phase grating, in Bragg conditions, is given by:

$$\eta = \sin^2(\Delta\delta_{vol}/2) = \sin^2(\pi n_1 d / \lambda \cos\theta) \quad (1.11)$$

where n_1 is the amplitude of refractive index modulation, d is the thickness, λ is the incident wavelength, θ is the incident angle. Under suitable conditions a Bragg grating can reach a diffraction efficiency η of the order of 100%. On the other hand, when $Q < 1$ the grating is said to be thin and it corresponds to the Raman-Nath regime of the optical diffraction. In this regime, many diffraction orders can be observed. These gratings are also characterized by a low selectivity concerning the angle of incidence. The efficiency of the first-order Raman-Nath diffraction, in a grating with a sinusoidal modulation of refractive index, is given by:

$$\eta_{surf} = J_1^2(\Delta\delta_{surf}/2) = J_1^2\left(\frac{2\pi d(n_1)}{\lambda \cos\theta}\right) \quad (1.12)$$

where $J_1^2(\Delta\delta_{surf}/2)$ is the first-order Bessel function of the first kind, d is the depth of the gratings grooves and n_1 is the amplitude for the refractive index modulation. According to the properties of the Bessel function, the maximum diffraction efficiency η is $\eta_{max} = 33.9\%$. This classification, made by using the Cook-Klein parameter, is valid only in the limit of low refractive index modulation³, otherwise other restrictions have to be imposed. In fact, for

³It means that the refractive index modulation amplitude has to be small compared to

large modulation even a “thick“ grating can present multiple diffractive orders [38, 39].

1.5.1 Holographic Polymer Dispersed Liquid Crystals

Between the the last 80s and the early 90s some groups of researchers understood the great potentiality of the employment of PDLC materials in the field of holography [1, 2, 40, 41]. In 1989 the first PDLCs based gratings, operating in the Raman-Nath regime, were realized [42, 43]. The work of Sutherland and his collaborators on PDLC gratings (usually referred to as H-PDLC) continued [1, 2, 44, 45], showing the possibility of realizing, with a fast and cheap technique, high efficiency and electrically switchable gratings. The interest for this kind of structures grew up: both from the point of view of basic research [46, 47] and application in display technology [48], switchable optical devices [49], photonic crystals [9, 10, 50–52], lasing [53–55], and sensors [56]. The technique exploited is the PIPS (discussed in chapter 1.3); the used materials are sensitive to a particular light wavelength, so that the phase separation can be driven by laser light. For a typical PDLC, LC droplets are randomly distributed in the polymer matrix and the droplet axes are randomly oriented, while in H-PDLC system, the interference of two beams generates periodic dark and bright fringes in the photopolymer film. The inhomogeneous curing of the prepolymer mixture brings to the formation of LC droplets richer regions alternated to polymer richer regions [57]. The resulting structure presents a refractive index modulation, which can be modified by applying an external stimulus. Many H-PDLC systems show a polarization dependence of the optical properties, which can be related to the choice of materials [58], to shrinkage effects [59, 60], or to a particular process of fabrication [61, 62]. In these sys-

the average refractive index

tems a certain degree of orientational order of the NLC droplet axes is present, but in the most general case droplet axes are randomly oriented, so that the light propagating through the structure will experience an index modulation that does not depend on the polarization of incident light.

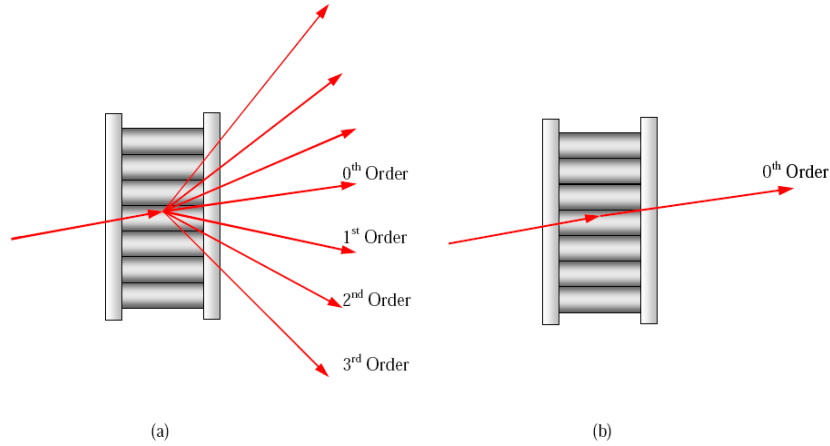


Figure 1.11: a) On state of an HPDLC, any field is applied b) Off state of an HPDLC

By exploiting an external field, the droplet axes can be oriented along a unique direction. If one of the index, usually n_o matches the polymer binder index a completely switchable modulation can be realized. When the index modulation is turned off by the application of an external field, the diffraction efficiency of the grating vanishes.

1.6 POLICRYPS Gratings

The optical properties of H-PDLC devices strongly depend on the presence of LC droplets inside the gratings. In fact if the droplet size of NLC is comparable with the wavelength of the impinging light, this is strongly scattered. It is necessary, therefore, to reduce the average size of the nematic droplets in order to obtain high diffraction efficiency and low scattering losses [63]. In

this case, however, the switching electric field becomes rather high (15-20 V/ μm) [64]. In the last years, an attempt has been made to fabricate a new kind of holographic gratings [5] that exhibits better optical qualities. These gratings consist of polymer slices alternated to films of regularly aligned NLC (the name is POLICRYPS, acronym of POLymer LIquid CRYstal Polymer Slices). Besides the quality of the obtained morphology, a visible confirmation of the absence of NLC droplets in the POLICRYPS structure is reported in fig.1.12, where it is shown the presence of disclination defects inside fringes occupied by NLC molecules [65]. This kind of texture defects are usually pertinent only with a continuous nematic phase.

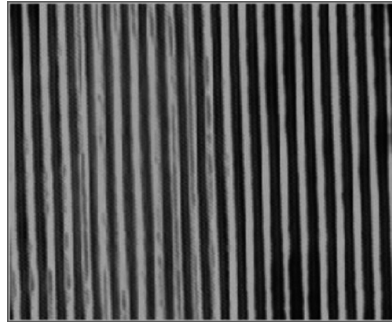


Figure 1.12: Optical microscope picture of a POLICRYPS grating. The dark lines present in the liquid crystal channels are disclinations in NLC director

The basic idea for the fabrication of POLICRYPS is to avoid the formation of the Nematic phase during the curing process. In this way, an almost complete redistribution of NLC and monomer molecules inside the sample is induced, by exploiting the high diffusion which the NLC molecules can undergo only when they are in the isotropic state. The realization of POLICRYPS gratings is therefore result of a new technique, called MPTIPS, from the acronym of Mixed Polymerization Thermal Induced Phase Separation. The standard procedure consists of the following steps:

- Heating of a sample of photo-initiator - monomer - NLC mixture up to

a temperature which is above the Nematic-Isotropic transition point of the NLC component. This step prevents the appearance of a nematic phase during the curing process;

- Illumination of the sample with the interference pattern of a curing UV radiation;
- Slow cooling of the sample below the Isotropic-Nematic transition point (typically, down to the room temperature) after the curing radiation has been switched off and the polymerization process has come to an end.

This general procedure is resumed in Fig.1.13

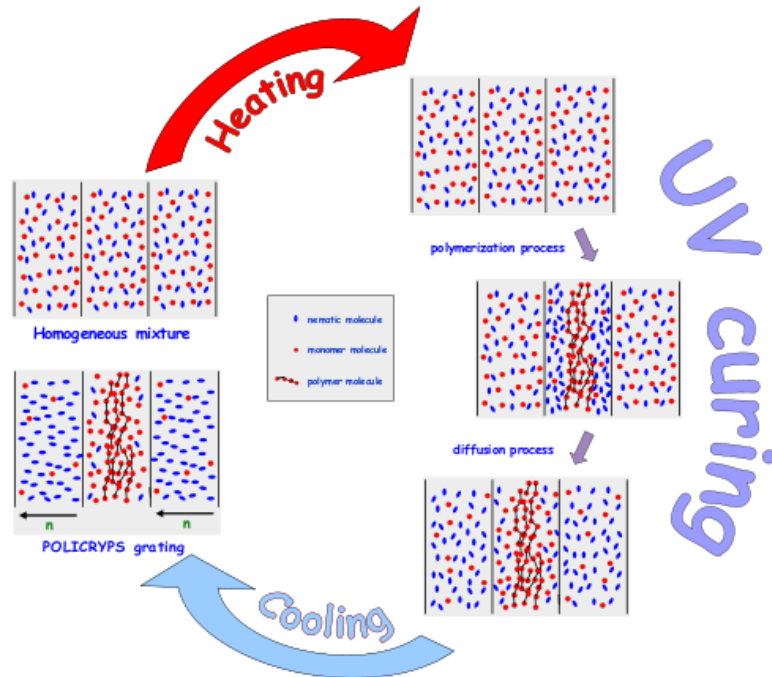


Figure 1.13: Sketch of POLICRYPS gratings production procedure. The diffusion of the involved species is increased by curing the gratings at a temperature which is above the N-I transition point of the used liquid crystal material.

POLICRYPS gratings have been fabricated mainly by using UV laser sources for the curing process. The initial syrup, as reported in literature [66],

is prepared by diluting a Nematic liquid Crystal (usually 5CB or BL-001 (E7) by Merk) in the pre-polymer system Norland Optical Adhesive NOA 61. The concentration of liquid crystal is around 30% of the total blend. Varying the geometry of the optical writing set-up, a grating spacing that reaches the micrometric scale has been obtained. Diffraction efficiency can reach really high values, the highest reported one being around 98%. Characteristic switching voltages vary in the range 1-5 V/ μm , and in general they decrease with temperature and with the initial NLC concentrations. [66]. In fig. 1.14 there is an interesting comparison between two Bragg gratings obtained from the same initial syrup and in the same experimental conditions, except for the curing temperature: one of them (HPDLC) is cured at ambient temperature, the other one (POLICRYPS) is cured at a temperature above the nematic-isotropic transition point [5]. Differences in the morphology and in the electro-optical properties show the importance of the role played by the temperature of the system during the curing process.

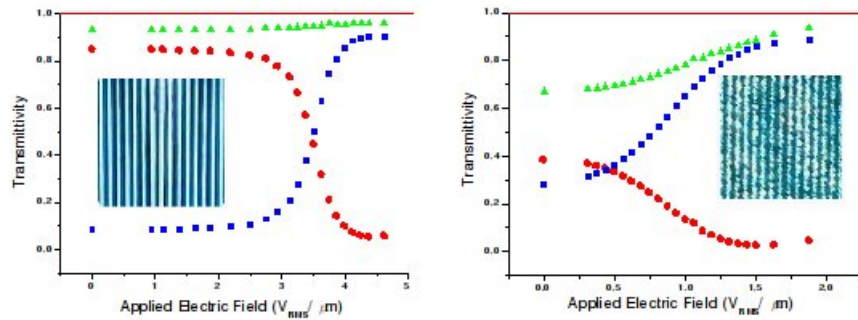


Figure 1.14: Electric field dependence of zero-order transmittivity (squares), first order transmittivity (circles), total transmittivity (triangles) for: (a) POLICRYPS grating and (b) HPDLC grating at room temperature. Picture in the inset shows a typical POLICRYPS and HPDLC grating morphology with the same spatial period, respectively

The good NLC alignment in the grating channels, make them really sensitive to light polarization. This characteristic enables realization of devices that exploit the NLC birefringence, such as phase modulators, based on the POLICRYPS fabrication technique [67], which proves, in general, a good solution for the realization of holographic optical devices; therefore POLICRYPS gratings has been used for different applications [68]. The possibility of extend the method to two dimensional structures or in general to other geometry has not been explored, except for the two step process developed in [69].

1.6.1 A model for POLICRYPS and HPDLC formation

In this section we discuss an existing model [57] which explains the mechanisms at the base of the formation of POLICRYPS gratings. The system under study is a syrup of pre-polymer and NLC acted on by the interference pattern of an electro-magnetic field. The model takes into account both chemical and mass diffusion processes occurring during the curing. Considering a sample of length L in z direction and infinite in x and y direction, filled with a mixture of liquid crystal, monomer and initiator in concentration C , M , I respectively; the sample is acted on by two intersecting and coherent plane waves, whose wavevector is along x . A classical reaction scheme for polymerization is considered [26] and a conventional Fick diffusion is assumed for mass transfer processes. With the aid of assumptions reported in [70] the whole process is driven by the following coupled equations:

$$\frac{d\mu}{d\tau} - B \frac{\partial}{\partial \xi} \left[(1 - \nu)^{\frac{2}{3}} \frac{\partial}{\partial \xi} \left(\frac{\mu}{1 - \nu} \right) \right] + (1 + m \sin \xi)^{\frac{1}{2}} \mu = 0 \quad (1.13)$$

$$\frac{d\nu}{d\tau} - \frac{G}{2} (1 + m \sin \xi) \left[N_0^2 (1 - \gamma) + N_0 (1 + \gamma) + \frac{2\gamma}{1 - \gamma} \right] \gamma^{N_0} = 0 \quad (1.14)$$

$$\frac{d\sigma}{d\tau} - B \frac{\partial}{\partial \xi} \left[(1 - \nu)^{\frac{2}{3}} \frac{\partial}{\partial \xi} \left(\frac{\sigma}{1 - \nu} \right) \right] = 0 \quad (1.15)$$

The system is written in a reduced form, which enables an immediate insight into the features of the investigated phenomena: $\sigma = \frac{C}{T}$, $\mu = \frac{M}{T}$ and $\nu = \frac{P}{T}$ are the relative concentrations of components (C, M and P stand respectively for the liquid crystal, monomer and polymer concentration, while T for the total molecular concentration), the variable instead $\tau = \left(\frac{k_p}{k_t} \sqrt{k_t g W(x) I} \right) t$ is a dimensionless time; k_p and k_t are the chemical prolongation and termination constants for the polymer formation reactions, and t is the time. The local intensity of the curing pattern is given by $W(x) = W_0(1 + m \sin qx)$, where $W_0 = I_1 + I_2$ is the total intensity (I_1 and $n_I I$ are the refractive indices of the adjacent areas of the grating. I_2 being the intensities of the two interfering beams) and $m = 2 \frac{\sqrt{I_1 I_2}}{I_1 + I_2}$ is the fringe contrast. Furthermore, $q = 2\pi/\Lambda$, where Λ is the fringe spacing, and $\xi = qx$.

B, G and γ stand for

$$\begin{aligned} B &= \frac{4\pi D k_t^{\frac{1}{2}}}{(g W_0 I)^{\frac{1}{2}} \Lambda^2} & G &= \frac{(g W_0 I k_t)^{\frac{1}{2}}}{k_p T} \\ \gamma &= \frac{\mu}{\mu + G \sqrt{(1 + m \sin \xi)}} \end{aligned} \quad (1.16)$$

Here D is the monomer diffusion constant and g represents the activation probability of the initiator molecules when acted on by the radiation. N_0 stands for the least number of monomer molecules which are needed for the

formation of an immobile polymer chain; by means of this parameter, we can account for a spatial modulation of the sample properties even in the particular case of a single component initial mixture.

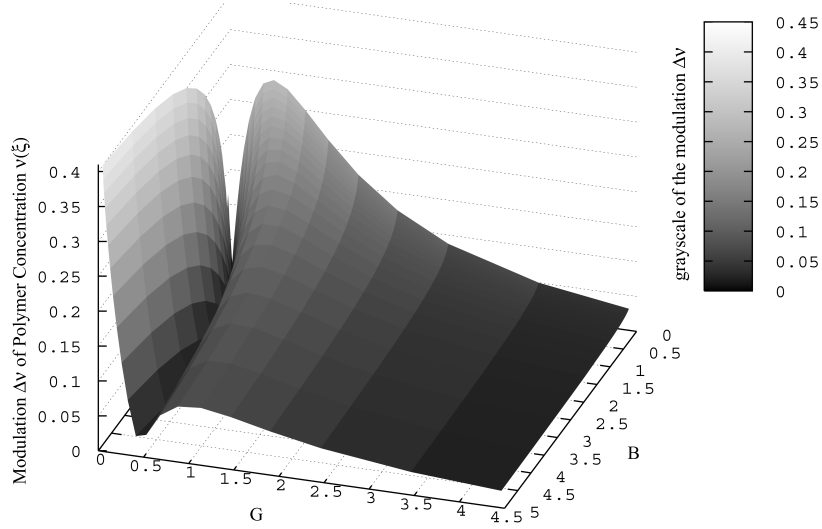


Figure 1.15

In the interpretation of results obtained by exploiting this model recognize two different regimes. The first, indicated as fast curing regime, refers to a polymerization process which is faster than diffusion, so that polymer chains grow before monomer diffusion take place. In the second regime, indicated as slow curing regime, the polymerization reaction is slow enough to enable monomer molecules to diffuse across the fringes before they react (slow curing). Figure 1.15 is concerned with the main features of this model: The modulation $\Delta\nu$ of the polymer concentration across the fringes indicates the degree of phase separation and is an important parameter that determines the diffraction efficiency of the grating. It is calculated as the first Fourier component of $\nu(\xi)$ [70]. The surface indicating $\Delta\nu$ is plotted as a function of B and G parameters for $N_0 = 4$ and shows that two regions of high $\Delta\nu$ values are present; this means that there are two possible ways of obtaining high diffraction gratings. For

$B \ll 1$, the polymerization reaction is very fast in comparison with diffusion. Starting from a uniform distribution of initiators and monomers, when the radiation creates a high number of radicals in the bright fringes, for these molecules it is more probable to recombine and form a new initiator molecule, than to meet monomers and form a long polymer chain. On the other hand, the low number of radicals created in the dark fringes can capture a great number of monomers before a chain is closed; this corresponds to the fast curing case.

$G \ll 1$ with $B > 1$ means $k_p \ll k_t$. In these conditions it is more probable for a chain to be closed by a radical than to get a new monomer. There is no difference in chain length between dark and bright fringes and, because of the great number of available radicals, polymerization takes place mainly in the bright fringes. For $G \gg 1$ and $B \gg 1$ we have a high impinging intensity and a noticeable diffusion: The curing process becomes quite homogeneous and there is no modulation of the polymer concentration. As already said, the curing process of POLICRYPS occurs in a high diffusive regime, this situation is described by the model for a high value of B , and a low value of G . Experimental results are in good agreement with the model [6, 66, 68]. Moreover equations 1.16 show that B and G parameters are directly related to grating formation parameters such as the curing intensity, the grating pitch and the temperature of the system. The model can be therefore used as a guide for POLICRYPS gratings realization.

1.7 SLM Technology

The optimization of a new holographic technique for the realization of 2D periodic or a-periodic structures can be interesting for many applications. Dif-

ferent methods exist for the realization of two dimensional holographic structures. For example, the multi-beam interference method allows the reproduction of even complicated 2D and 3D photonic structures, but its main disadvantage is the difficulty in the realization of a stable and well balanced optical set-up; Indeed, in the multi-beam method intensity and stability of each interfering beam must be under control. Another possibility is the use of photo-masks, realized with other methods, such as e-beam lithography. In this case, however, diffraction effects due to the light interaction with the edges of the photomask can affect the quality of the recording pattern. During the work of thesis, we decided to utilize a single-beam technique that involves the use of a programmable Spatial Light Modulator (SLM). The instrument enables realization of different 2D periodic and aperiodic light patterns maintaining the same single-beam set-up. SLMs are essentially two dimensional programmable transparencies capable of controlling the wavefront of an incident light beam. Initially used as purely amplitude- or intensity-based display technologies, SLMs have found new phase-based applications in adaptive optics [71], holographic projections [72] and optical tweezers [73]. Phase-based SLMs produce phase variations by changing the path length of the incoming beam either by variation in the refractive index or in the medium thickness. Liquid Crystal On Silicon (LCOS) is the most prominent technology used for the realization of SLMs. LCOS is a reflective microdisplay technology based on a silicon backplane; the backplane is used to electronically address and interface with individual aluminum pixels covered with a liquid crystal layer. The aluminum acts both as an electrode and a mirror, allowing optical interaction with the liquid crystal layer, which is typically composed of NLC. The light wave passing through the material will see different refractive indexes depending on NLC director orientation relative to the electric field component

and to the direction of propagation. Therefore phase modulation is achieved according to the director alignment in each pixel, which is driven by voltages applied through the electrically addressed backplane.

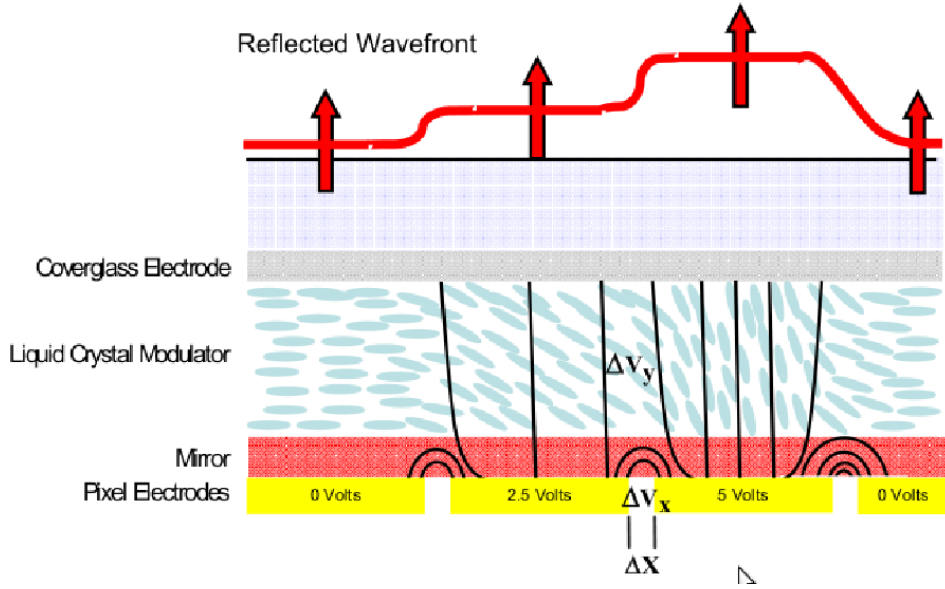


Figure 1.16: This is the section of a typical reflecting spatial light modulator. In the sketch i shown how a different applied voltage can change the phase retard introduced by each pixel.

In this work we used a reflecting phase only Spatial Light Modulator, (Pluto-VIS LCOS by Holoeye), controlled by a computer exactly as an external monitor. It can be easily addressed with a bitmap image in gray scale (256 levels); each gray level corresponds to a phase delay in the interval $[0-2\pi]$. The challenges related to the realization of the desired holographic pattern, via SLM, are essentially two: The first one is the calculation of the right phase function to be charged on SLM in order to obtain the reconstruction of the desired intensity distribution. The second challenge is the implementation of an optical set-up for the reproduction of a light pattern with the desired magnification. An further problem that has been solved is related to the incompatibility of the used instrument with an UV curing. The UV light is very

reactive with a lot of materials and impose the use of dedicated optics . The first effort was the individuation of the right materials and of the experimental conditions for the realization of a POLICRYPS visible curing. In fact, the POLICRYPS technique has been optimized only for pre-polymer mixture sensible to the UV light. In the next chapters we will treat the problematics related to these points and we will discuss in details the chosen strategy.

Chapter 2

POLICRYPS visible curing

The phase-only SLM (Pluto-VIS by Holoeye) cannot be exposed to UV light: It is operative only in the wavelengths range between 400 nm-600 nm; therefore beside the study of the pattern generation by SLM our efforts were focused on the individuation of the proper materials for the POLICRYPS visible curing. We decided to use as a light source a Nd:YAG laser doubled in frequency, emitting a light wavelength of 532 nm. The properties required for the pre-polymer mixture are the efficiency and the good balance between the polymerization rate and the diffusion of the different components. The first requirement is due again to a limitation in the use of the SLM, in fact the maximum power supported by the instrument is 2 W/cm^2 . The photo-curing has to be efficient enough in order to guarantee the start of the process with a relatively low light intensity. The second requirement is necessary for the accomplishment of the POLICRYPS technique. In order to achieve a complete phase separation the liquid crystal must diffuse across the system before the gel-point¹ is reached. Otherwise the liquid crystal is captured in droplets as small as the polymerization rate is fast. When we introduced the POLICRYPS technique (chap. 1) we said that the high temperature can assure a high diffusive

¹at the gel-point we have the first appearance of the polymer network

curing regime, but also the materials involved and their reciprocal interaction can strongly influence the diffusion properties of the system. The considerations of the second point suggested us to put aside one of the most common pre-polymer mixture used for the visible curing of h-pdlc systems [1]. It is composited by a blend of the monomer Di-Pentaerithrol Hydroxy Penta Acrylate (DPHPA), the commercial nematic liquid crystal E7, the chain extender N-Vinyl Pyrrolidone (NVP), the initiator dye Rose Bengal (RB) and the coinitiator N-Phenyl Glycine (NPG). The DPHPA precursor is composited by multi-functional acrylate monomers that undergo a free-radical chain polymerization. In fact, because of the fast polymer growth rate, it is widely employed in the realization of h-pdlc gratings. A fast polymerization and a highly cross-linked network are important to get very small LC droplets (typically 100 nm) and consequently a negligible light scattering. These properties makes this material suitable for fast and efficient hpdlc formation, but inadequate for the POLICRYPS curing. Thus we considered a different class of monomers based on thiol-ene polymerization. A detailed treatment of thiol-ene polymerization mechanisms is present in ref. [74,75]. The polymer precursor we used is a commercially available Norland Optical Adhesive (NOA61), designed for the UV curing. The exact chemical composition of NOA resins is proprietary; anyhow through the studies conducted on these materials we know that it a mixtures of polyfunctional urethane based thiols and allenes [76,77]; These resins undergo a free-radical step-growth polymerization. Thus, they are characterized by a slower curing rate that makes them better candidates for POLICRYPS curing.

2.0.1 Pre-polymer mixtures tested

In order to test different pre-polymer mixtures we realized a simple two beams interferometric set-up (fig.2.1). The one dimensional gratings realized have a

period of $10\mu\text{m}$. The sample is a glass cell filled at room temperature with the pre-polymer mixture. The glass used presents a thin conductive coating of ITO (Indium Tin Oxide). The cells preparation has been conducted entirely in the clean room of the Licryl lab (UNICAL). The procedure followed for the sample preparation is reported:

- The glass is first cut in rectangular pieces ($2\times 2\text{ cm}^2$, $1.5\times 3\text{ cm}^2$)
- The glasses are sonicated in a solution of NaOH
- The NaOH residuals are washed away by with distilled water only
- The glasses are dried with nitrogen or warm air
- The glasses are stuck together with a UV sensible resin, containing silica spheres spacers with a diameter of $10\mu\text{m}$.
- The cells are exposed to the light of a UV lamp to stimulate the resin hardening
- The cells thickness is measured with a spectrophotometer.

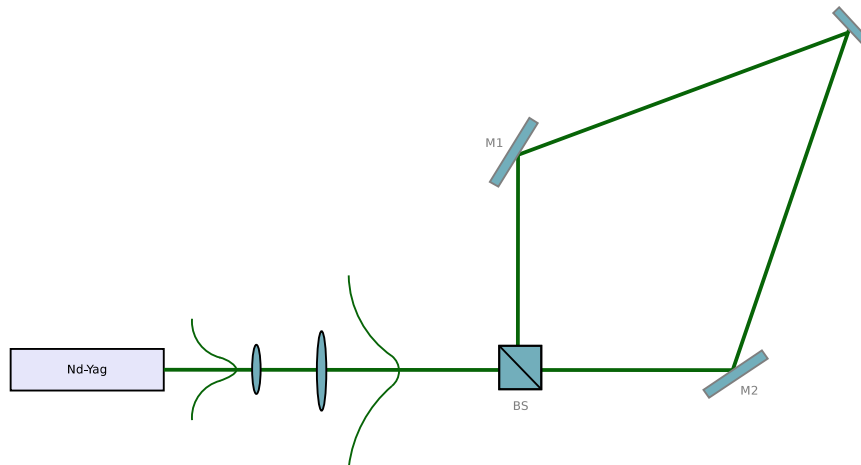


Figure 2.1: Interferometric set-up

The composition of the first pre-polymer mixture tested is reported in table 2.1.

Table 2.1: "Pre-polymer mixture 1"

Component Type	Component Name	Percentage
Monomer	NOA-61	65-70%
Liquid Crystal	E7	28-30%
Initiator	RB	1%
Co-initiator	NPG	1%
Solubilizer	NP	1-6%

The monomer has refractive index n_p ($=1.56$) very closed to the liquid crystal ordinary index n_o ($=1.52$); the liquid crystal birefringence is equal to 0.2. The index match is a necessary condition if we want that a complete reorientation of the molecules correspond to the switch off of the gratings diffractive properties. The RB-NPG couple of photo-initiators is a tested system [1]. The absorption of a photon by the photoinitiator RB results in an excited singlet state followed by fluorescence or inter-system crossing to the triplet state. The RB triplet undergoes an electron-transfer reaction in which NPG functions as an electron donor, producing an NPG radical.

The addition of the reactive diluent NVP is necessary for obtaining a uniform syrup. The monomer precursor NOA61 isn't a good solvent for the two photo-initiators. Moreover the diluent NVP is composited by mono-functional monomers that can participate to the polymerization process, thus it can be considered as a cross-linking agent also. Its behavior is not yet completely understood even if in a "series of works" its influence on the phase separation mechanisms in hpdlc systems is reported [78–80]. The combinations of the two actions of NVP as cross-linking agent and solubilizer inhibits NLC

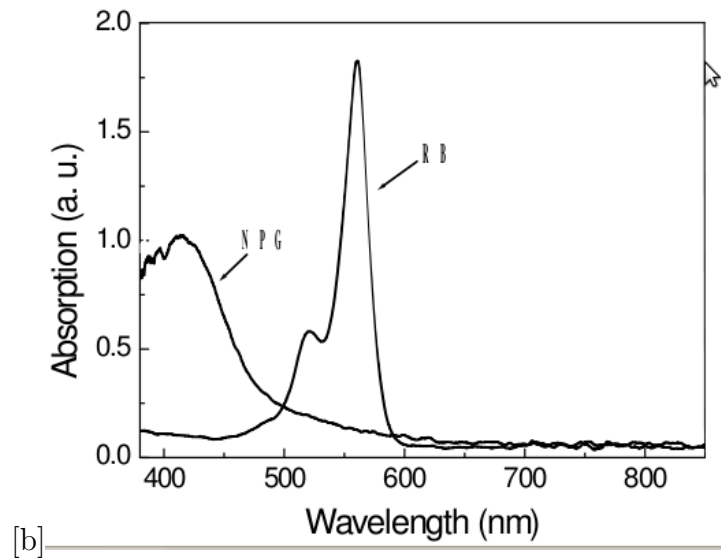


Figure 2.2: Absorption spectrum of RB and NPG photo-initiators

phase separation, bringing to the formation of reduced-size droplets. In our experiments we used NVP percentages under the 6% wt. The support that hold the sample is maintained, during the curing, at a constant temperature of 60 ± 1 °C. The single laser beam intensity has been varied between 1 – 15mW. The experiments were characterized by long curing times (10-20)min. Even in the system studied the phase separation dynamics and the resulting grating morphologies are strongly influenced by the presence of NVP. The gratings realized are characterized by polymers walls alternated to liquid crystal regions, in which the liquid crystal doesn't form a continuous phase but it is trapped in a tangled polymeric net.

The presence of NVP prevent the possibility of a POLICRYPS morphology. For our second attempt we chose a mixture with a small number of elements, the monomer, the liquid crystal and a titanocene photoinitiator.

It's commercial name is Irgacure 784. It has an absorption peak near (440-460) nm, but a little absorption around 532 nm (fig.2.4b).

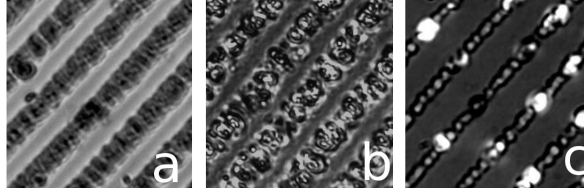


Figure 2.3: Samples cured in the same experimental conditions, with a different % of NVP in the initial blend: a)6% wt b)3% c)1%. Both extension of the liquid crystal regions and droplets size vary with the NVP concentration.

Table 2.2: "Pre-polymer mixture 2"

Component Type	Component Name	Percentage
Monomer	NOA-61	68-70%
Liquid Crystal	E7	28-30%
Initiator	Irgacure784	1-2%

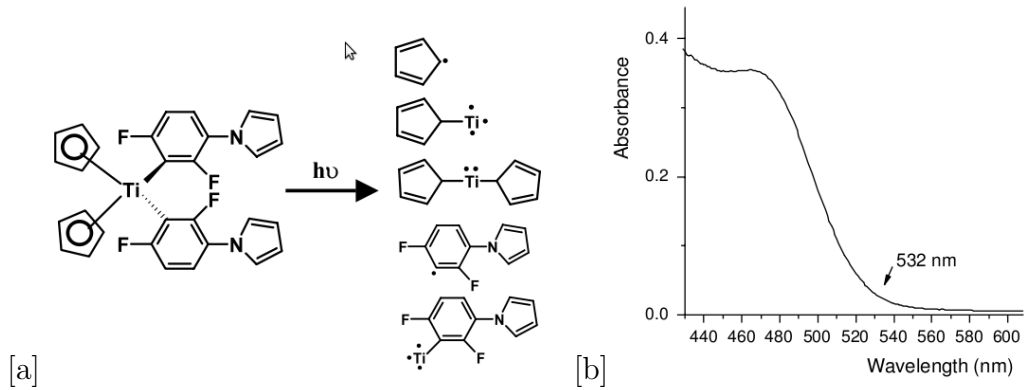


Figure 2.4: a) Typical absorption spectrum of Irgacure784 in NVP as a solvent
 b) The molecular structure and photo-dissociation of the Irgacure 784 molecule

Recent work demonstrate that, despite this low absorption, efficient photo-polymerization processes can be triggered by the photoinitiator for an exciting wavelength of 532 nm [81]. In fact each titanocene molecule yields four radicals and thus an enormous concentration of free radicals can be produced in a short time (fig.2.4b). In our system the initiation of the process is due

to the interaction of irgacure 784 with the UV photoinitiator already present in noa61 resin [82]. Combining the photo-polymer system described and the POLICRYPS technique we succeeded in obtaining diffraction grating characterized by the alternation in space of polymer and liquid crystal slices.

2.0.2 1D Raman Nath Gratings

Here is reported the characterization of POLICRYPS gratings realized using the titanocene photo-sensitive mixture. A curing intensity of 10 mW for each recording beam has been used. The curing process takes place at a temperature of 60°C and it keeps 20 min. At the end of the recording a slow cool down assures a good liquid crystal alignment. Due to the construction parameters (Equ.1.9) the grating realized have a multi-beam diffractive behavior. The typical diffraction efficiency of the gratings is around the 20%. The good phase separation and the liquid crystal alignment in the channels is proved by the observation of the gratings between cross polarizers (fig. 2.5).

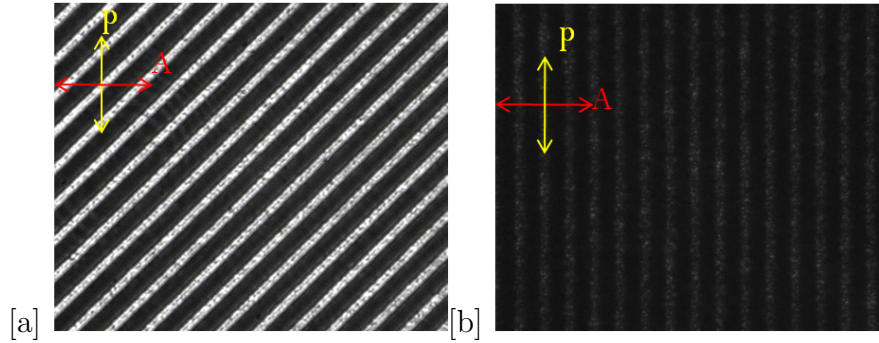


Figure 2.5: Optical microscopic pictures of a grating making 45° (a) and 90° (b) with polarizers

The nematic director of the NLC confined in the channels is perpendicular to the polymer walls. When the NLC director \mathbf{n} makes an angle of 45° with the polarizer axes the light transmission trough the analyzer reaches its maximum.

When \mathbf{n} is perpendicular to the polarizer direction no changes in the polarization of the light propagating through the sample are introduced; thus there is no light transmission between cross polarizers. The reason of the liquid crystal alignment in POLICRYPS is still under investigation by looking for into the nematic polymer walls interactions, also responsible of the POLICRYPS switching behavior [7]. A further confirmation of liquid crystal alignment is given by the dependence of the zero and first order diffraction transmittivity on incident light polarization.

A set-up (fig.2.6) for the gratings characterization has been realized. In

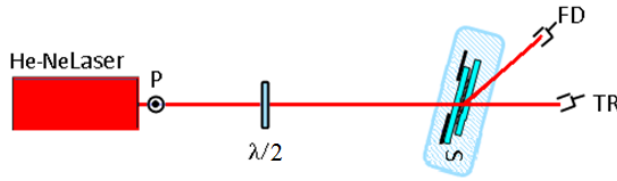


Figure 2.6: A half-wave plate rotates the polarization of the laser beam without attenuating its intensity. Two photodiodes connected to two different channels of an oscilloscope collect the light of the zero and the first diffracted orders

figure 2.7 the typical polarization behavior of our diffraction gratings is shown. The diffraction efficiency reaches its maximum value when the polarized light sees the effective refractive index n_e for the liquid crystal. On the contrary the signal is almost turned off when the polarization sees the refractive index n_o . In fact the polymer index is chosen to match the value of n_o . The behavior of the zero order is obviously opposite.

As we explained liquid crystal based gratings are dynamic optical elements. The NLC order can be changed or disrupted with a consequent change in the diffraction properties. In figures 2.8, 2.9 two different ways for switch off the diffraction efficiency of our gratings is shown. In fig. 2.8 is reported the variation of the diffraction efficiency for a probe with polarization s, and a

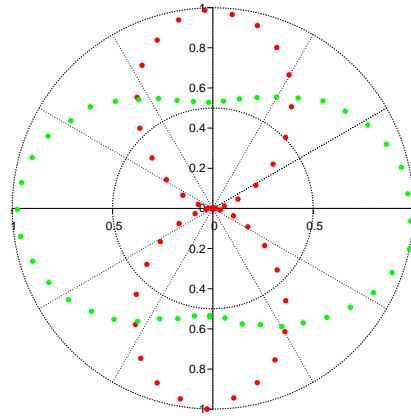


Figure 2.7: The green dots are related to the transmitted order, the red dots are related to the first diffracted order

probe with polarization p for different temperatures of the system.

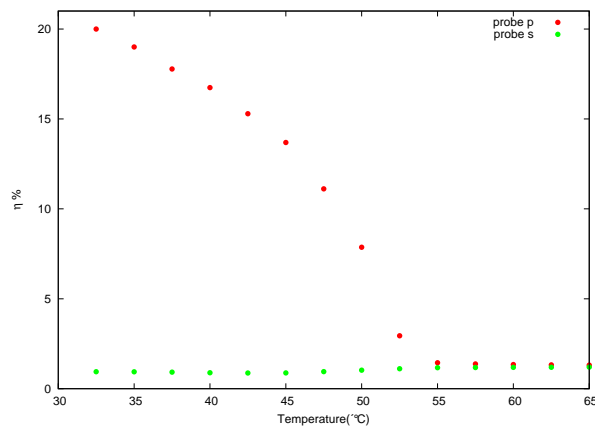


Figure 2.8: Probe s, Probe b

The diffraction efficiency for the p probe decreases with temperature and vanishes after the threshold of 55°C due to the transition of NLC molecules to the isotropic state. The threshold value in the POLICRYPS system is slightly lower than in the pure nematic. The presence of impurities such as residual short chain or unreacted photoinitiator can perturb the orientational order of the molecules. The polarization s remains almost constant, the average refractive index seen by this polarization is almost the same both in the ordered

and in the disordered system. We studied also the response of the gratings to the application of an external electric field. The figure 2.9 is a typical electric switch. A square waves with a frequency of a 700 Hz, has been applied to the cell. The set-up is very similar to the one in fig.2.6, but this time the sample is electrically connected to a function generator. We applied a modulated signal in order to avoid screen effects².

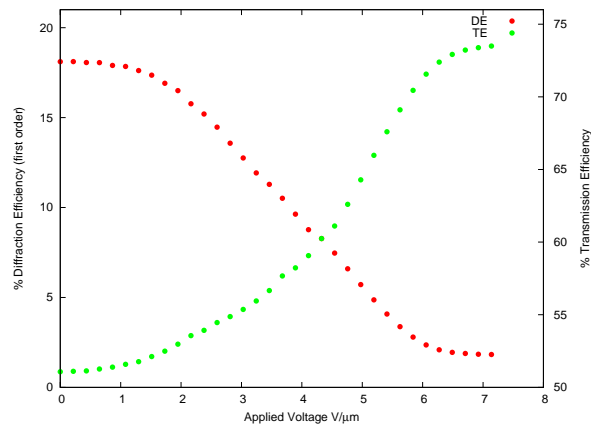


Figure 2.9: Probe s, Probe b

The switching properties of these gratings are very similar to the one documented for POLICRYPS gratings obtained with a UV curing. The voltage required for a complete switch, the response time and the restore time are the typical of POLICRYPS gratings [5].

Table 2.3: "Response Times"

Falling time	Rising Time
700-800 μ s	1-3 ms

²Due the presence of free charge in the system, the application of a static field can create a charge accumulation with the consequent formation of an opposite screening field

Chapter 3

Pattern Generation via computer holography

If suitably addressed, a Spatial Light Modulator can modify the wavefront of an impinging electro-magnetic wave, thus producing the desired diffraction Fraunhofer pattern. Such two-dimensional intensity distribution can be used for photo-curing purposes. On the other hand, the optical lenses ability to perform the Fourier Transform of an field allows to obtain a magnified copy of this pattern in the focal plane of a lens system [83].

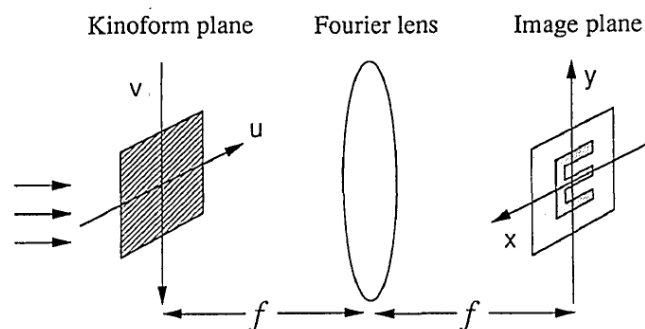


Figure 3.1: Image reconstruction in the Fourier plane

SLM technology has been developed in the framework of diffractive optical

elements (DOE) design¹, and it offers an easy and innovative solution for real time phase implementation. In our treatment, light is considered in terms of the scalar theory of diffraction [84, 85]; it is monochromatic, coherent and it is described by the complex function of two spatial variables. The module and the argument of this complex function are called amplitude and phase of the light field. The light field emerging from a generic optical element can be described as the product between the initial light function and the transmission function associated to the optical element. The phase transfer function associated to SLM consists in the complete set of phase delays introduced by each pixel in the complex field, it can be called kinoform, computer generated hologram (CGH) or DOE's phase. In general, the kinoform, cannot be directly calculated from a desired arbitrary intensity profile. The phase retrieval is actually a challenging problem and in literature it is referred to as an "ill-posed inverse task" [86]. Phase hologram synthesis is opposite to the usual diffraction problem, in which the diffraction object is given and the diffracted field is sought. Indeed it concerns a problem of inverse scattering in which the diffracted image is prescribed and the diffracting object (the hologram) is sought. Impropriety of the problem of synthesis lies in the fact that, first, there may not be a solution; second, if the solution exists it may be non unique; and third, the solution may be unstable.² Therefore, the problem of kinoform synthesis can be regularized by replacing the desired image with a similar one, such that the solution exists and it is stable. When an exact solution is unknown, a widely used method for kinoform calculation is the implementation of an Iterative Fourier transform algorithm (IFTA) [86]. An IFTA predicts the

¹A Diffractive optical element is defined as a device designed and realized to have a given optical transfer function. It can be realized as microrelief surface or transparency.

²A solution is said unstable when small deviations of the phase function from the calculated one may result in considerable degradation of the formed image.

propagation of a beam through an initial kinoform by fast Fourier transform (FFT), and then successively modifies the kinoform based on a comparison between the predicted and desired focal plane intensities. In this work, a C^{++} iterative code based on a modified IFTA has been realized. The next chapter will discuss in more details the algorithm scheme.

3.1 IFTA implementation and results

Iterative Fourier Transform Algorithms have been introduced in the 70s [87,88] and till now experts in computer generated hologram technology and light manipulation are continuing to develop their advanced versions [89–91]. In this work, two C^{++} codes based on two different algorithms have been realized: the Gerberg Saxton (GS) [87] and a modified version of an Adaptive Additive (AA) algorithm [86], called Mixed-Region Amplitude Freedom (MRAF) [91]. An IFTA, in general, is a technique able to solve the following problem: design a CGH that will convert a light field $A_0(u, \nu)$ at the CGH (input plane), into a target intensity distribution $I_t(x, y)$ at the focal plane of a focusing optics (output plane). The IFTA problem does not have a unique solution, as the complex phase of the optical field associated to $I_t(x, y)$ is not constrained. Thus, there is a choice of phase in the output plane, known as phase freedom. An IFTA is designed to use phase freedom to minimize the difference between $I_t(x, y)$ and the intensity distribution produced by the CGH in the output plane. An IFTA can be decomposed into two parts as illustrated in fig.3.2: an initialization step and an iterative loop. In the initialization step, a phase distribution $k_0(u, \nu)$ is chosen as a starting point for the algorithm and it is imprinted on $A_0(u, \nu)$ to produce the input field $E_{in}^{(1)}(u, \nu)$. At each iteration n , the input field $E_{in}^{(n)}(u, \nu)$ is propagated to the output plane by using a Fourier

transform (eq.2 of fig.3.2). Then the produced light intensity $I_f^{(n)}(x, y)$ (eq.5 fig.3.2) is compared with the target intensity by calculating a figure-of-merit ε (eq.6 fig.3.2). The last step included in the iteration is the calculation of a new input field $E_{in}^{n+1}(u, \nu)$ (eq.4 fig.3.2) to be used in the next iteration. The iterative loop is terminated after N iterations, once ε does not improve with repeated iterations. The phase profile $K_f(u; \nu) = \text{arg}(E_{in}^{(N+1)})$ of the field in the input plane for the final iteration is the kinoform which must be transferred to SLM.

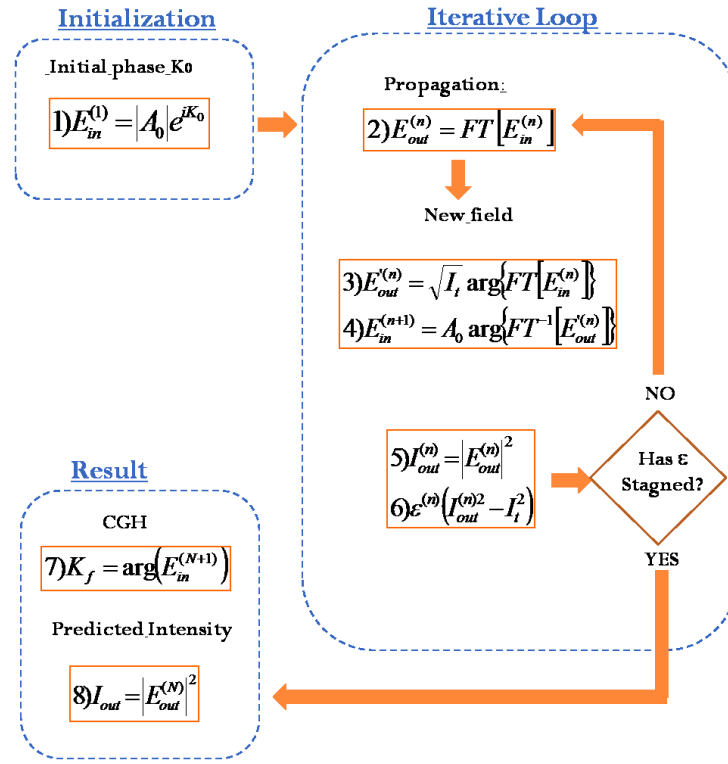


Figure 3.2: Gerberch-Saxton algorithm scheme

The convergence parameter chosen (ε in the scheme of fig.3.2) is a root mean square error (MSE) based on the difference between target and calculated output intensity (eq.3.1).

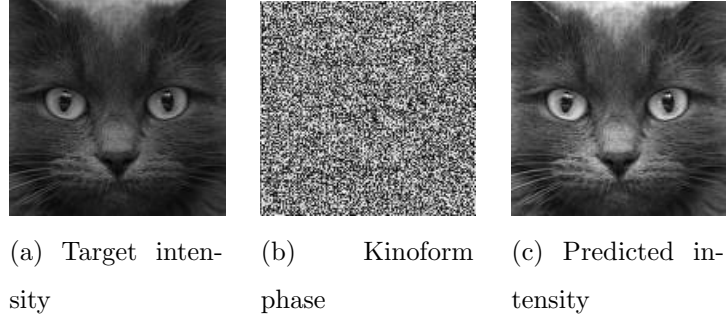


Figure 3.3

$$MSE^{(n)} = \sqrt{\frac{1}{N \times M} \sum_{(x,y)} \frac{[I^{(n)}_f(x,y) - I_t(x,y)]^2}{I_t(x,y)^2}} \quad (3.1)$$

At each iteration the MSE is calculated and compared with the one calculated for the previous iteration. When the difference between the two becomes smaller than a prescribed value ξ , the loop is stopped. ξ values tested for the GS algorithm go from 10^{-6} to 10^{-12} . The number of iterations is of the order of 10 till $\xi \leq 10^{-8}$; then, getting smaller value of ξ , hundred iterations are required. The choice of the initial phase is also important: a smooth varying phase can avoid the onset of vortex stagnation problems, typical of random phases [91, 92]. Indeed the presence of jumps in the initial phase generates phase singularities in the kinoform, which correspond to zero intensity spots in the output plane. IFTAs are not able to overcome the problem, thus further iterations do not bring a real improving of the image leading, instead, to a stagnation [93, 94]. The quality of reconstructed images has been measured by using MSE associated to other parameters, like the roughness value ρ (eq.3.3), or the only MSE.

In fig. 3.3, some results obtained by using the C^{++} code based on GS algorithm are presented. The target intensity is a 200x200 pixel gray scale image; a spherical phase has been used as initial step. The kinoform shown

in fig. b has been calculated by imposing $\xi = 10^{-8}$; the number of iteration is 25. The MSE value calculated in this case is 0.3. The GS algorithm is able to reproduce any generic distribution of intensity, as shown in the figure 3.3. Anyhow, the attention of this work is focused on realization of binary intensity distributions, thus we considered a different IFTA version called MRAF. The main difference between GS and MRAF algorithms is the way in which the new input field is generated at the end of each iteration. The Gerberch Saxton algorithm described in the scheme of fig.3.2 first calculates a new output field by eq.3 of fig.3.2, then it calculates a new input field by eq.4 of fig.3.2. MRAF presents a different expression for the new output field. Following this approach eq.3 of the scheme in fig.3.2 is substituted by the following equation:

$$E'_{out}{}^n(x, y) = [m \cdot A_t(x, y)|_{SR} + (1 - m) \cdot A_{n_{out}}(x, y)]arg[FT(E_{in})|_{NR}] \quad (3.2)$$

where $A_{out}^n(x, y)$ is the amplitude associated to the previous output field and m is a mixing parameter that can be varied to optimize the algorithm convergence. The MRAF algorithm is designed to reconstruct images where a region with zero intensity can be distinguished from a signal region. Indeed, the new field is a sum whose terms are calculated on different regions of the output plane: noise region (NR, the region of zero intensity) and signal region (SR). As in the Adaptive Additive algorithms, besides phase freedom, also amplitude freedom is considered, but in this case the amplitude freedom is allowed only in the noise region. This algorithm is characterized by a higher accuracy, confirmed by lower roughness values.

Results of reproduced MRAF code are shown in fig.3.4. The imposed ξ value is 10^{-12} . The same experiment has been performed by using the GS algorithm in the same conditions (initial phase, ξ value, convergence parameter ε). In fig.3.5 a comparison between the two algorithms is shown, MSE and ρ values

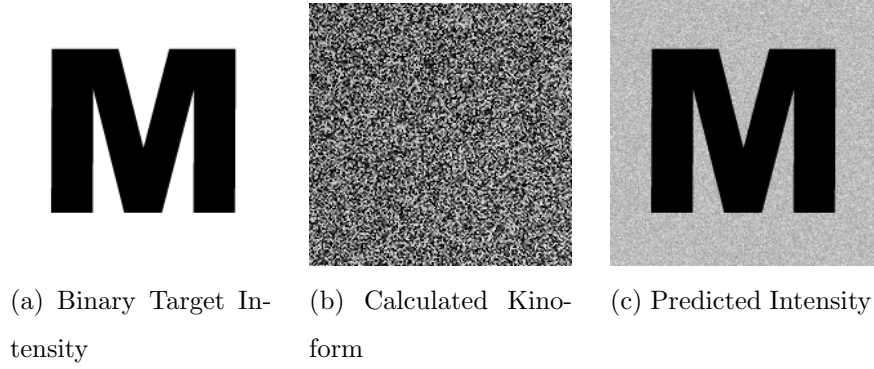


Figure 3.4

are also reported. Roughness ρ has been evaluated, in signal region only, by equ. 3.3

$$\rho = \sqrt{\sum_{SR} \frac{(I_{out} - I_{out})^2}{NxM}} \quad (3.3)$$

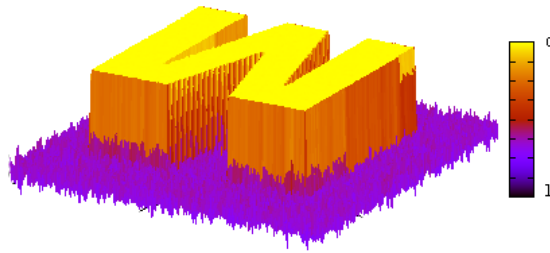
where NxM is the signal region area.

In fig.3.5 a) and b) a 3D plot for the predicted intensity calculated by GS and MRAF algorithm are presented, respectively roughness values are $\rho_{GS} = 0.58$ and $\rho_{MRAF} = 0.43$. The MSE error are instead $MSE_{GS} = 0.3$ and $MSE_{MRAF} = 0.24$. The MRAF algorithm presents better values for the considered parameters, but a significative improvement of the algorithm performance can be obtained only by associating the mixed region strategy to a suitable choice of the initial phase [91].

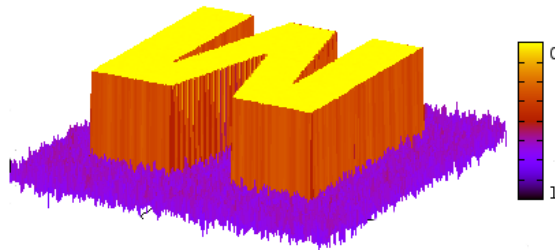
3.2 Limitations

Suitable light patterns for holographic realization of diffraction gratings are characterized by a high number of lines; from the point of view of image reconstruction, this means the necessity to reproduce fine details and a large pattern area. In Fourier optics, the complexity of a band-limited light signal³

³a band-limited signal are characterized by a Fourier Transform that is non zero only in a finite region of the frequency space



(a) image reconstructed by the GS algorithm based code



(b) image reconstructed by the MRAF algorithm based code

Figure 3.5:

is given by its space-bandwidth product, defined as the number of samples required to properly describe the signal. If the signal is non zero in the interval $-L_x \leq x < L_x$, $-L_y \leq y < L_y$, it is sampled, according with the Whitter-Shannon sampling theorem⁴, in a lattice with spacing $(2B_x)^{-1} (2B_y)^{-1}$ along

⁴The WS theorem says that the highest frequency that a system can reproduce cannot overcome the smallest sampling division. Said X and Y the division spacing in x and y direction respectively and B_x and B_y the widths of the frequency domain: the frequencies spectral range result determined also $X \leq (2B_x)^{-1}$ $Y \leq (2B_y)^{-1}$

x and y direction respectively. The space-bandwidth product is:

$$SBP = 16L_xL_yB_xB_y \quad (3.4)$$

It is evident that the necessity to reproduce a minimum number of grating periods and in the mean time ensure high spatial frequencies is problematic with an instrument characterized by a limited resolution (number of pixels). Only signals (images) whose SBP is supported by SLM can be properly reconstructed. Another problem that has to be taken into account is the CGH efficiency; only a portion of the incident light is diffracted into the reconstructed image, the rest being partially redirected into higher diffracted orders and partially transmitted. On the other hand, an upper limit for the diffraction efficiency of diffractive optical elements exist and it does not depend on the designing algorithm [95], but it is due both to spatial [96] and phase [97] quantization. In SLMs an important contribution to undiffracted light is given by the presence of an inactive area in the display screen. Indeed this “dead area” does not participate in the beam apodization, but it still reflects light.⁵ As indicated in fig3.6, each pixel is surrounded by a dead frame of thickness $\frac{\Delta d-d}{2}$: considering the whole SLM surface this “dead area” forms a lattice that reflects light, thus producing a pattern made by many diffracted orders [98,99]; the zero order is superimposed to the image reconstructed in the output plane. In order to eliminate this undesired zero order light, many solutions have been proposed [100,101], but all of them present some drawbacks.

Since the kinoform is an on-axis hologram, the zero order remains overlapped to the reconstructed image (fig.3.7a). They can be separated by shifting away the reconstructed image from the optical axis by adding to the kinoform

⁵In SLMs of last generation the presence of the “dead area” is reduced; it is usually indicated with the fill factor parameter that is the percentage of active area covering SLM total surface. Fill factor are usually > 80%

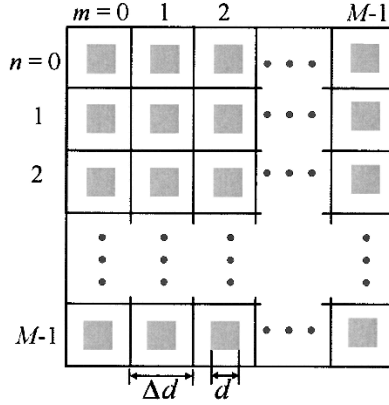


Figure 3.6: SLM display. The dark gray square inside each pixel is the active area.

a linear phase $\omega = \frac{2\pi}{p1}$ (fig.3.7b). This result can be explained by recurring to the statements of the Fourier transform shift theorem (eq.3.6)

$$FT(E(x, y)) = E'(u, \nu) \quad (3.5)$$

$$FT(E(x - a, y - b)) = E'(u, \nu) \exp[-i2\pi(au + b\nu)] \quad (3.6)$$

The produced shift has a cost in terms of functional and diffraction efficiency, moreover the illumination is not uniform and comatic aberrations can be introduced into the off axis reconstructed image [101]. Another solution is to introduce a lens correction by adding a quadratic phase $\omega = \frac{2\pi}{\lambda f}(u^2 + \nu^2)$ to the kinoform, where f is the focus of the equivalent lens. As a consequence, the reconstructed image is focalized into a different plane. This time the out-of-focus zero-order beam appears as a background noise in the light projection plane (fig.3.7c). The solution proposed by Palima [101] is to include into kinoform a supplemental phase information, thus producing a light beam able to interfere destructively with the zero order. In this case, however, part of SLM resolution, otherwise dedicated to the image reconstruction, must be used for this purpose.

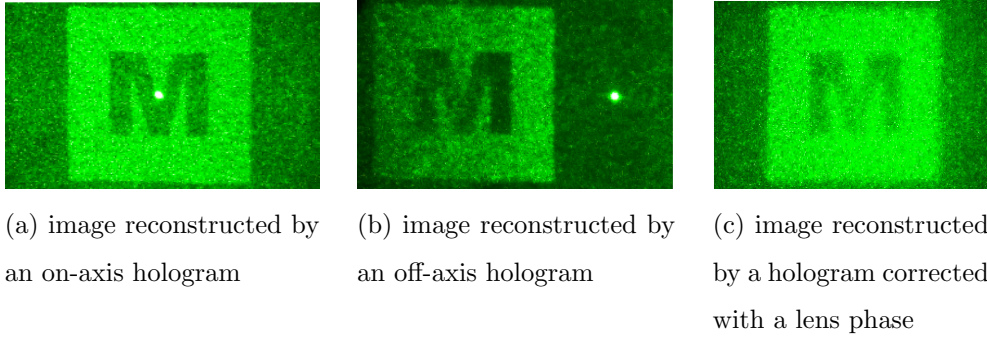


Figure 3.7: The three picture are produced by the GS based code with an error of $\eta = 10^{-8}$

Chapter 4

Periodic and aperiodic structure realized by direct imaging

4.1 From indirect to direct imaging

In the previous chapter it has been explained how to generate a pre-given intensity light distribution, by controlling the phase transfer function of a phase-only spatial light modulator. It has been highlighted how the number of pixels contained in a commercial spatial light modulator is not sufficient when the desired target intensity is a light pattern characterized by a high number of periods. Moreover solutions required to optimize image reconstruction by computer holography often need a further exploitation of SLM resolution. Pluto SLM total resolution is indeed 1920x1080 pixels, but the effective resolution used for kinoform implementation is lower:

- Only square images can be reproduced. In the Fourier plane, pixel size is determined by $l_x = \frac{f\lambda}{L_x}$, $l_y = \frac{f\lambda}{L_y}$, where f , λ and L_x , L_y indicate the focus of the lens system, the light wavelength and the physical dimensions of kinoform respectively. If $L_x \neq L_y$ the reconstructed image turns out to be distorted.

- The corrections devoted to zero order removal have also a resolution cost.
- The calculation time for large images can be important. The discrete Fourier Transform is performed by using a Fast Fourier Transform [102] and for a total of $N_X N_Y$ points it requires $N_X N_Y \log_2(N_X N_Y)$ additions and complex multiplications. The calculation is faster if the total number of point is a multiple of two: it is not an obligatory choice but for large size images it could be convenient.

A further approach that enables the full exploitation of SLM resolution has been considered. The image is not reconstructed in the Fourier plane, but in the object plane. Methods that allow imaging in the object plane are usually referred to as “direct”, in contraposition with the “indirect” methods that allow image reconstruction in the Fourier plane. In literature, some examples of direct imaging techniques exploitable by using SLMs are reported [11, 103]. The approach used in this thesis is really simple and it is based on a well known effect. A 4f set-up ¹ allow a magnified reproduction of the desired pattern in the object plane.

4.1.1 Edge enhancing effect

The direct imaging method used in this PhD work is based on the solution proposed by Davis in in 1989 to the problem of edge-enhanced response from a binary SLM, exploited as a phase only filter in pattern recognition applications [104]. Let us Consider a reflecting SLM: when an input image like the one show in fig4.1(a) is charged on SLM display, the output image is an edge enhanced

¹it is a classical set-up used in Fourier optics for image reconstruction. It is called 4f, that stay for 4 focal lenghts, because the object, the image reconstruted and two lenses of equal focus stay at a reciprocal distance of f . In the set-up used in this thesis the two lenses have $f_1 \neq f_2$

version (fig.4.1(b)). The only zero intensity region is limited to the letter edges. In order to produce a letter characterized by a zero intensity region within the letter frame the input of fig 4.1(b) is substituted by its randomized version 4.1(c). The randomization operation corresponds indeed to an edge enhancing operation: the image is replaced with a version consisting in a large number of edges due to the random pattern. Unlike binary SLM, which possess only two phase levels, the SLM modulators used in this work has 256 different phase levels; thus, the zero intensity region in the output image is better reproduced.

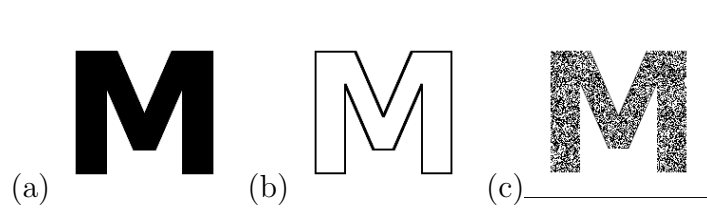


Figure 4.1: a) input image b) Edge enhancing version produced c) Randomized input

This technique allows the realization of any generic binary pattern, characterized only by two intensity levels. The images charged on SLM are the alternation of areas composed by pixels of the same color (white for example) alternated to randomized areas. Monochromatic and randomized areas in the input plane produce bright and dark areas in the output plane respectively.

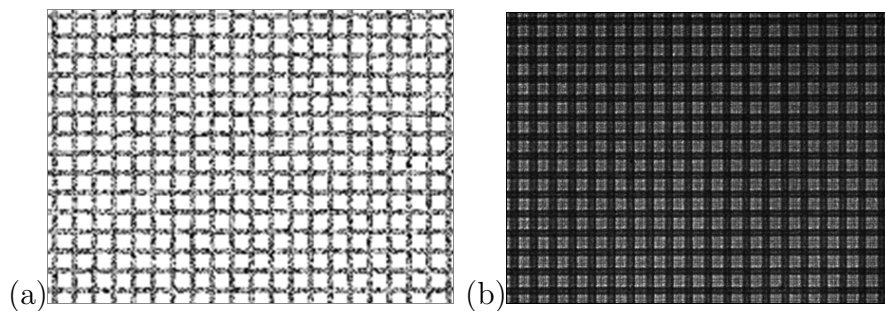


Figure 4.2: a) randomized input b) Output acquired by a beam profiler camera

In figure 4.2 a typical pattern is shown. The image b) is acquired by using

a beam profiler camera. In order to obtain a magnified pattern a 4f Fourier lenses system has been reconstructed. The two focal length f_1 and f_2 reproduce the magnification $M = \frac{f_2}{f_1}$. In figure 4.2 an enlarged and collimated beam is reflected by SLM, then it is magnified and relayed to the sample plane.

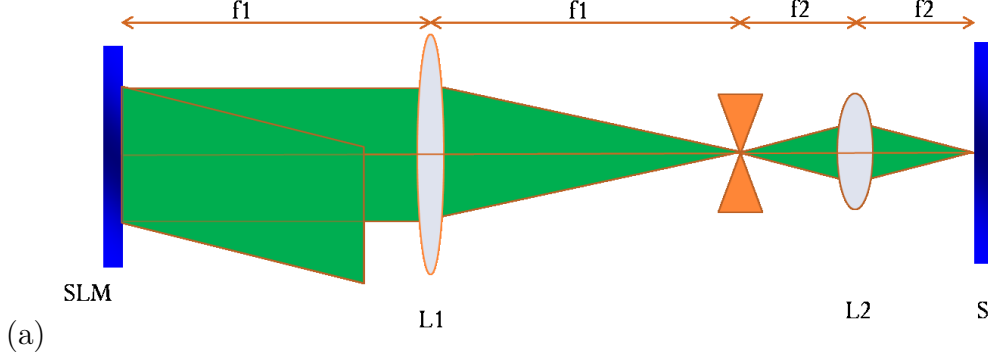


Figure 4.3: 4f Fourier set-up for image reconstruction

4.2 1D Raman Nath grating

1D Raman-Nath POLICRYPS gratings have been realized by using the set-up of fig.4.3, where the two lenses have focal Lengths $f_1 = 25cm$, $f_2 = 5cm$. The first experiments have been made by using input images composed by randomized and monochrome stripes of the same width. The typical morphology obtained is shown in fig 4.4: it is characterized by NLC stripes where liquid crystal is accumulated at the edges.

A Stripe width ratio, $\Delta d_m / \Delta d_r$ (where Δd_m and Δd_r are the monochrome and randomized stripes widths), which reproduces the real monomer-liquid crystal percentage ratio, favors a better phase separation. In the policryps curing process, polymer stripes are formed in correspondence of bright fringes, while liquid crystal stripes are formed in correspondence of dark fringes [57]; the sample volume interested by dark and bright fringes, is proportional to

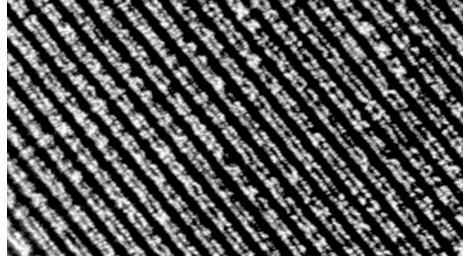
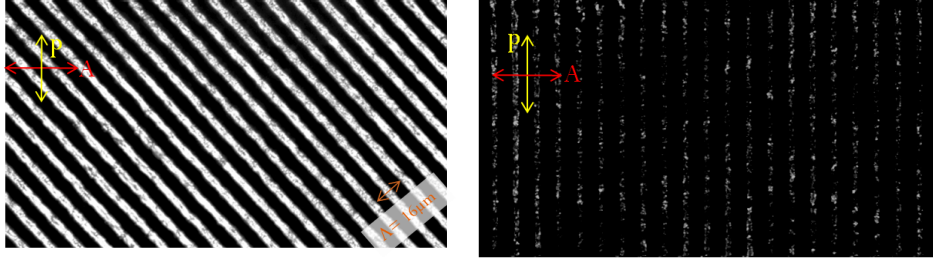


Figure 4.4: The grating has been realized by using a bitmap image in which randomized and monochrome stripes have the same width

the stripes width. The used pre-polymer mixtures is characterized by a 28-30% wt of liquid crystal, 68-70 % wt of monomer; thus the width ratio chosen is: $\Delta d_m/\Delta d_r = 7/3$. In this case the induced phase separation is complete and it produces a regular morphology. On the other hand, the liquid crystal percentage cannot be changed of a big amount, otherwise the POLYCRIPS formation is compromised. The NLC percentage in the pre-polymer mixture has a treashold value of 30% wt; if it is overcome liquid crystal forms droplets before polymerization process comes to an end, thus preventing a complete phase separation. Two optical microscope pictures (fig.4.5) of a sample rotated between cross polarizers show a liquid crystal preferential alignment perpendicular to polymer walls.

This characteristics of POLICRYPS gratings has been already observed in the 1D Raman Nath gratings realized by standard two beams interference. This is proved also by diffraction efficiency measurements performed by varying the probe polarization (fig. 4.6). The set-up used is the same of fig.2.6.

The observed switching behaviour is typical of POLICRYPS gratings realized by the classical interferometry technique. In fig.4.7, a switching curve for the grating realized by SLM is presented. The two curves refer to different probe polarizations. The applied electric signal is a square wave, with a frequency of $700Hz$. The grating can be switch on and off by means of con-



(a) NLC director forms a $\pi/4$ angle with the first polarizer direction (b) NLC director forms a $\pi/2$ angle with the first polarizer direction

Figure 4.5: Pictures acquired by optical microscope between cross polarizers. The grating spacing is $16 \mu\text{m}$, the total cured area is 5mm^2 . The used pattern reproduces the liquid crystal/monomer proportion

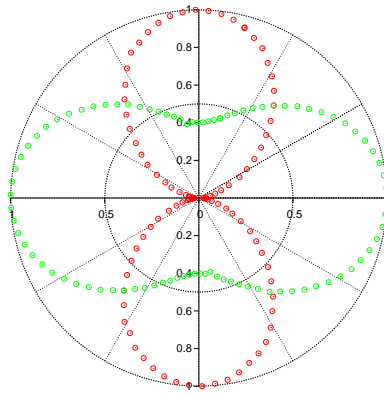


Figure 4.6: Green and red lines represent the normalized transmittivity for the zero and the first diffracted orders respectively. Maximum diffraction efficiency for the first order is 21%, while zero order maximum transmittivity is 74%

secutive impulse. The OFF state is reached in $800\mu\text{s}$, while the ON state is reached in 1-3 ms (the same reported in chapter 2).

The switching behaviour is well comparable with the one of 1D POLICRYPS realized by means of the standard interferometric technique.

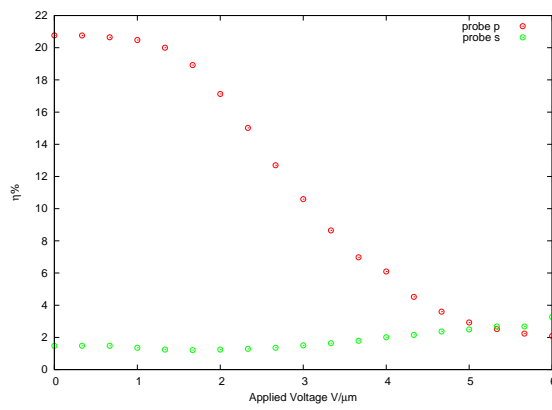


Figure 4.7: The green and the red line represent the diffraction efficiency for a p and a s probe polarization respectively.

Chapter 5

Periodic and aperiodic structure realized by direct imaging

5.1 2D Periodic gratings

One of the main advantages of using SLM to produce light curing patterns is the possibility to realize a serie of different 2D stuctures keeping the set-up untouched. Of the wide zoo of structures produced in this work, a few of them will be discussed and charaterized in this section to demonstrate how it is in fact possible to produce generic 2D POLICRYPS structures, once the main problems discussed in previous chapter and sections have been faced and solved.

The first presented example is realized using a regular grid of dark circular spots in a light background, as the light curing pattern to imprint on the photo-sensitive sample. The resulting structure presents a good phase separation, with the liquid crystal confined in cylinders, regularly distributed in a polymeric bind. In fig.5.1a,b the two optical microscope pictures of this sample rotated between cross polarizers are presented. The curing time of this sample is 20 min while the intensity is 10 mW/cm^2 . As a further confirmation of a

liquid crystal confinement in the cylinders it is remarkable that any polarization dependence of the diffraction efficiency of the structure has been observed. Structures realized by using shorter exposure times and higher intensities ex-

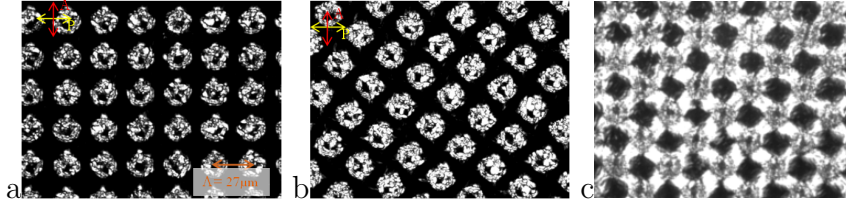


Figure 5.1: optical microscope pictures acquired between cross polarizers. The grating spacing is $27 \mu\text{m}$. In fig. c) an example of a structure in which liquid crystal is not confined in the cylinders, forming instead channels connecting adjacent cylinders

hibit a bad diffusion of NLC molecules: liquid crystal is present both in the background area and in channels connecting adjacent cylinders, thus resulting in a bad morphology (fig.5.1c). This is an evidence of the importance of determining the most suitable values of the POLICRYPS parameters.

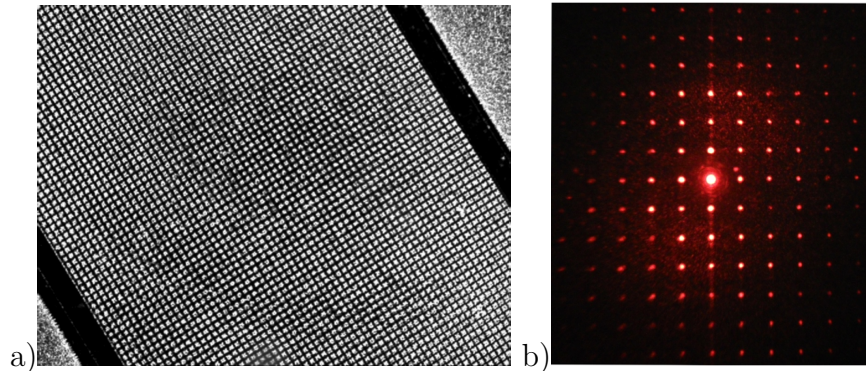


Figure 5.2: a) Optical microscope image of a larger sample area for the same sample of fig.5.1 a) and b). The total cured area is 5mm^2 . b) Far-field diffraction pattern generated by the structure

The structure of fig.5.3 is presented to discuss the confinement of liquid crystal in a 2D grid thus it has been fabricated using the light curing pat-

tern presented in fig.4.2. Once the structure is realized, the NLC molecular director appears to be perpendicular to the channel walls; this is confirmed by the measurement of diffraction efficiencies for 1-0 and 0-1 orders (fig.5.4b) for different probe polarizations. The two polar curves are indeed perpendicular to each other indicating that the NLC director in horizontal stripes is oriented perpendicular to NLC director in vertical stripes. As further proof of the

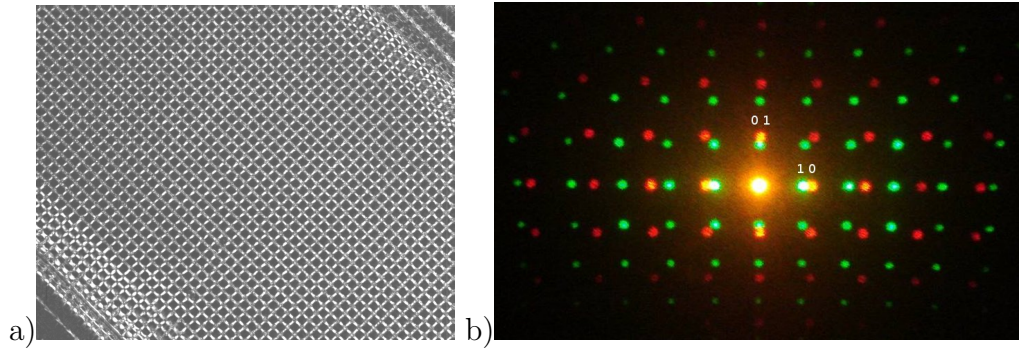


Figure 5.3: a) Optical microscope picture of a grid POLICRYPS. The grid spacing is $38 \mu\text{m}$, the total cured area is 5mm^2 b) Far field patterns of the grid produced by using a green (532 nm) and a red (633 nm) wavelength. The 1-0 order is produced by the vertical stripes, while the 0-1 order is produced by the horizontal stripes of the lattice

POLICRYPS nature of the realized structure, we remark that this 2D lattice presents a switching behaviour very much similar to the one of the Raman Nath POLICRYPS gratings discussed in previous chapters. In figure 5.4(b), the time dependence of diffraction efficiency is shown: a square wave, characterized by a frequency of 700 Hz and an amplitude of $5 \text{ V}/\mu\text{m}$, is applied in successive interval of 400 ms. The OFF state is reached in $800\mu\text{s}$, while the ON state is reached in 1-5 ms.

Finally, the complete phase separation, characteristic of the POLICRYPS morphology, is further proved by the presence of disclinations in the intersection between vertical and horizontal channels. In these regions, two different ori-

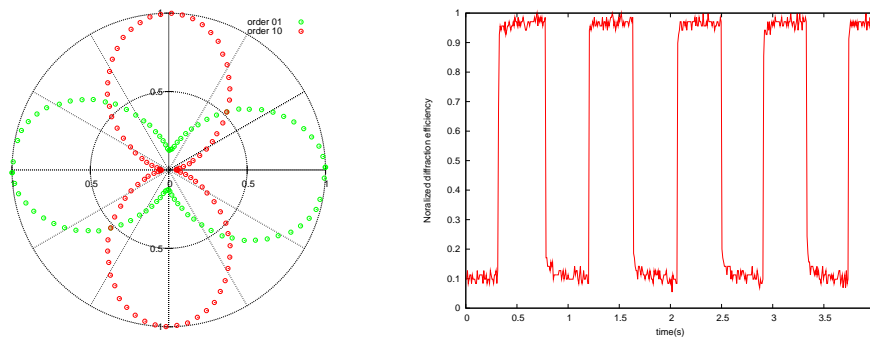


Figure 5.4: Polar plot of the diffraction efficiency of the structure of fig.5.3. a) The green polar curve is related to the 10 order, instead the red polar curve is related to the 01 order. The measured diffraction efficiency of the two orders is around 8%. b) Electric switching of 10 order is reported; the 01 order has exactly the same behavior. The diffraction efficiency is normalized to 1.

orientations for the molecular director intersect each other, creating a singularity in local nematic director orientation as illustrated in the sketch in fig.5.5. This feature can appear only if a pure nematic phase was present in the grid channels.

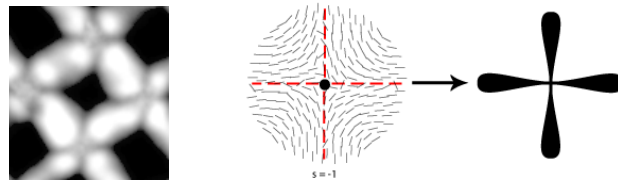


Figure 5.5: In fig. a) disclinations present in a lattice structure are shown b) a scheme that describes the disclination formation at the channels intersection. The darker cross present in fig a) and depicted in the scheme is the disclination appearance between cross polarizers.

Being realized only in the curing regime theoretically and experimentally demonstrated for POLICRYPS gratings and showing a good morphology, characterized by a complete phase separation and short switching times as well,

we can conclude that the realized samples are, in fact, 2D POLICRYPS structures.

5.2 Aperiodic structures: fork gratings

The main benefit of the exploited technique is that it can be used to realize asymmetric geometries, hardly realizable by using multi-beam interference. The fork grating phase illustrated in fig.5.6 is an example of how it is possible to conjugate advantages of both holographic and photo-curing technique: it is not realizable by exploiting multi-beam interference and it does not present singularity in NLC alignment and therefore disclinations defects. A fork grating is able to modify the wavefront of an incident Gaussian beam, producing a diffraction pattern composited by several optical vortexes (fig.5.7).

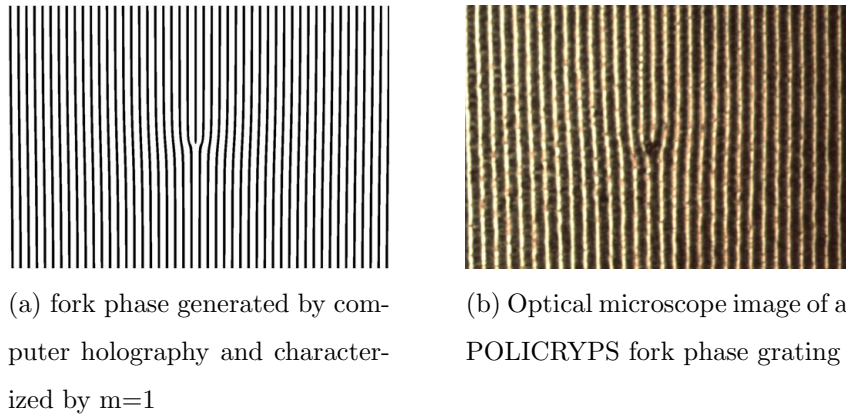


Figure 5.6

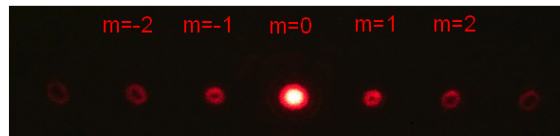


Figure 5.7: Far field diffraction pattern composited by switchable optical vortexes

An optical vortex is a light beam characterized by an helical wavefront described by phase function $\psi_1 = \exp(im\theta)$, where θ is the azimuthal angle of a cylindrical coordinate system (r, θ, z) where z is the light propagation direction. For the points belonging to the helical axis ($r = 0$), the phase is not defined and the corresponding light amplitude is zero, indeed an optical vortex projected on a screen appears like a ring with a zero intensity region in the center. The integer m present in ψ_1 expression indicates the number of phase winding around the dark spot.

Optical vortexes are widely used for optical trapping of microscopic dielectric particles. In conventional optical trapping, the Gaussian laser beam is used to trap those particles whose refractive index is greater than that of surrounding. However, due to a gradient in intensity and darkness near the center optical vortexes can trap both types of particles whose refractive index is greater or lower than the surrounding medium one. [105,106] The fork phase of fig.5.6(a) has been produced by computer generated holography by simulating the interference of two waves [107,108]: a reference beam and an object beam containing the vortex singularity. When a reference beam illuminates the CGH (computer generated hologram) the vortex is reproduced in the output plane. A plane wave ¹ $\psi_2 = \exp(ikx)$ interferes with the object beam described by ψ_1 generating an intensity distribution proportional to the CGH.

$$\psi_{CGH} = |\psi_1 + \psi_2|^2 = |\exp(ikx) + \exp(im\theta)|^2 = 2[1 - \cos(kx - m\theta)] \quad (5.1)$$

The plot of the calculated ψ_{CGH} for $m = 1$ produces the pattern in fig.5.6(a); the fig. (b) reproduces the POLYCRIPS structure realized by the direct holographic technique. The produced optical vortexes 5.7 can be easily

¹Near its optical axis the wavefront of a Gaussian beam can be approximated by a plane wave; in the experiments we used a Gaussian beam as a reconstructing beam

switched on and off by applying an external electric field. A complete characterization of the first diffracted order beam is reported below. In fig.5.8 a beam profiler acquisition of the first diffracted order is presented. Its intensity profile is like a Gaussian profile with a zero intensity region in the center.

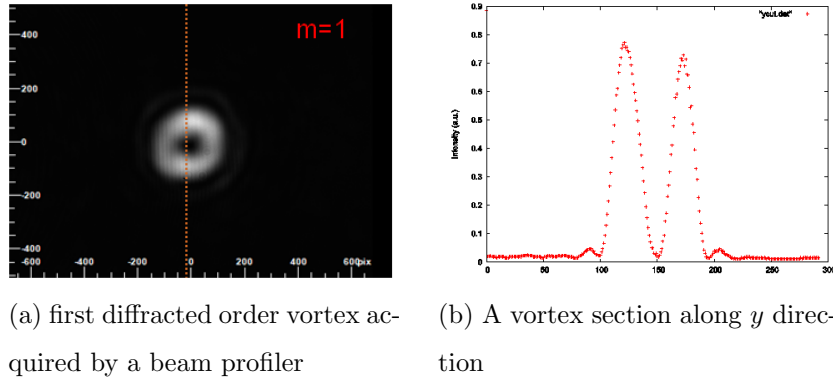


Figure 5.8

The polarization dependence of the first diffracted order vortex is shown in the polar graph of fig.5.9; Its switching behavior is presented in fig 5.9 (b)-(c). The voltage necessary to switch off the fork grating is $5V/\mu m$. Switching times necessary to turn off and on the structure are $t_{down} = 800\mu m - 1ms$ $t_{rise} = 4 - 6ms$ respectively. The applied voltage is a square wave signal with a frequency of 700 Hz.

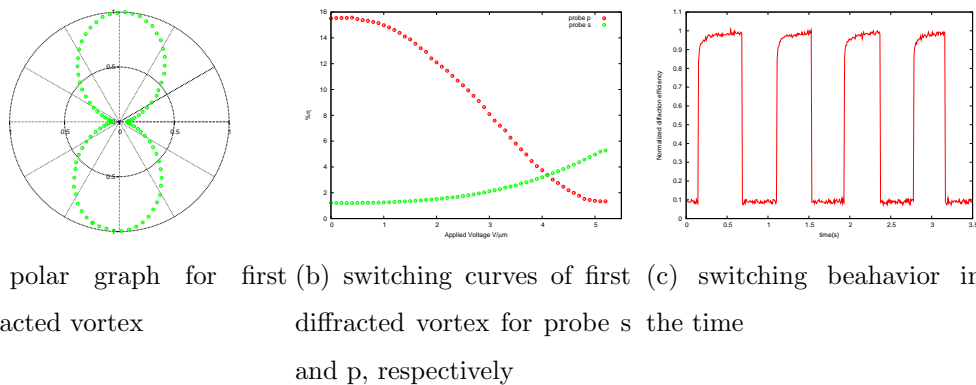


Figure 5.9

Chapter 6

Di-block copolymer confined in thin films

The interest in Block copolymers (BC) materials lies in their spontaneous micro-segregation in anisotropic domains [109–111]. Their self-assembling ability enables the preparation of structures whose periodicities (10-100 nm) are often not accessible by any other fabrication process. The possible applications of such technique are wide and diverse, in particular the work presented in this thesis was planned to be the starting section of a larger project, whose aim is the use of a lamellar di-block copolymer (D-BC) template for the organization of plasmonic nanoparticles. It is in fact possible to selectively gather nanoparticles in one of the two blocks during the segregation process by opportunely functionalize them through chemical treatments. Also, considering that the interest is in having the nanoparticles arranged in spatially ordered structures, a strategy to force a uniform and well aligned phase it has to be utilized: in general when micro-segregation happens in absence of constraints different domains are not aligned. The method chosen in the present work is the exploitation of D-BC behavior when they are confined in thin films. In this case, the alignment of the global phase is determined by the interaction

of the two blocks with the environment and with the substrate. The objective of this work is the study of D-BC alignment on suitable substrates. In this chapter we will also show the results obtained on silicon wafers by using two different annealing techniques.

6.1 Di-block Copolymer

The architecture of block copolymers can be controlled by synthesis procedures and it is possible to prepare di-block, tri-block and in general multiblock copolymers [109]. We focused our attention on the simplest case in which two distinct homo-polymers, conventionally termed A and B , are covalently linked each other. The most characteristic feature of D-BC is the strong repulsion existing between unlike sub-chains. Their phase behavior has been the subject of numerous theoretical and experimental studies over recent decades, and it is relatively well understood [112–115]. The thermodynamic equilibrium of a diblock copolymer is governed by two competing contribution to the Gibbs energy: an unfavorable mixing enthalpy and a favorable mixing entropy. At high temperatures D-BC forms a homogeneous melt, but when temperature decreases the two blocks tend to segregate due to their reciprocal repulsion¹ (fig.6.1), thus considering only system enthalpy the demixing process is favored.

However the demixing process is also accompanied by a reduction of entropy due to the fact that chain configuration becomes more constrained. The phase behavior of a D-BC can be represented by the diagram of fig.6.1. Here f is the volume fraction of one block, while χ , known as Flory-Huggins parameter, is a measure of the interaction energy between different blocks and

¹A macroscopic phase separation is prevented because of the strong covalent link connecting A and B

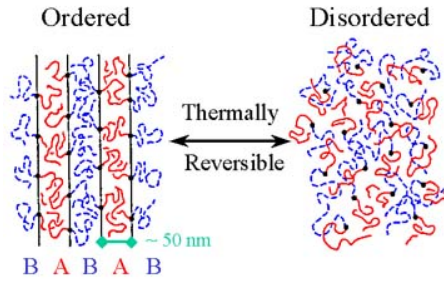


Figure 6.1

it decreases with temperature, $N = N_A + N_B$, instead, is the total degree of polymerization which is related to the configurational entropy. The product $\chi \cdot N$ indicates the degree of micro-phase segregation. The transition from a homogeneous melt of chains to a heterogeneous melt of ordered micro-separated domains is called order-disorder transition (ODT) and it occurs for a $(\chi \cdot N)_{ODT}$ critical value, depending on the volume fraction f . As indicated in fig.6.1, varying f , very different structures can be obtained. In this work a symmetric DBC has been used, f is around 0.5 and it corresponds to a lamellar phase, whose period is given by the block sequence A-B-B-A.

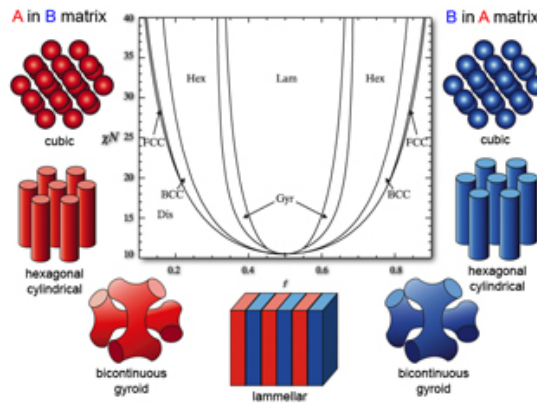


Figure 6.2: Theoretical phase diagram calculated for a generic DBC. The incompatibility is higher at low temperatures. (S) Spheres (C) Hexagonal (G) Gyroid (L) Lamellae

6.2 Thin film lamellæ organization

Nanoscale structures based on BC self-assembling offer a wide range of possibilities for applications: they can be used for high density data storage [116], for nano-lithography [117] and for the realization of hybrid materials [118], but for these purposes a fine control of their spatial order is necessary. The most efficient method for aligning BC in the bulk is the application of mechanical shearings [119, 120]. Electric fields have also been used [121] even if BC orientation in this case is less efficient. The realization of BC thin films is a powerful method that allow to control spatial orientation of BC structures [122, 123]. In contrast to the bulk, the morphology of amorphous BC thin films can be strongly influenced by surface and interfacial energies as well as the commensurability between the film thickness h and the period of the microdomains L . Also as predicted by Fredrickson [124] and experimentally proved by Anastasiadis [125] the presence of a surface can induce ordering in a copolymer system. Considering a lamellar D-BC a preferential interaction of one block with the substrate or a lower surface energy causes a segregation of that block at the substrate or at film surface. The connectivity of the blocks forces a parallel orientation of the microdomain to the substrate [123]. When the substrate is neutral, there is no preferential segregation of the components to the interfaces, therefore any perturbation can cause a perpendicular alignment of microdomains to the substrate. In case of a parallel alignment of lamellæ, two wetting behaviors are possible: a “symmetric wetting”, that occurs when one block segregates to both interfaces and an “asymmetric wetting”, that occurs instead when one block has a lower interaction energy with the substrate and the other block has a lower surface energy. Moreover in both wetting conditions the thickness of an ordered film h is not arbitrary, but it is defined in terms of L : in case of a symmetric wetting $h = nL$, while in case of

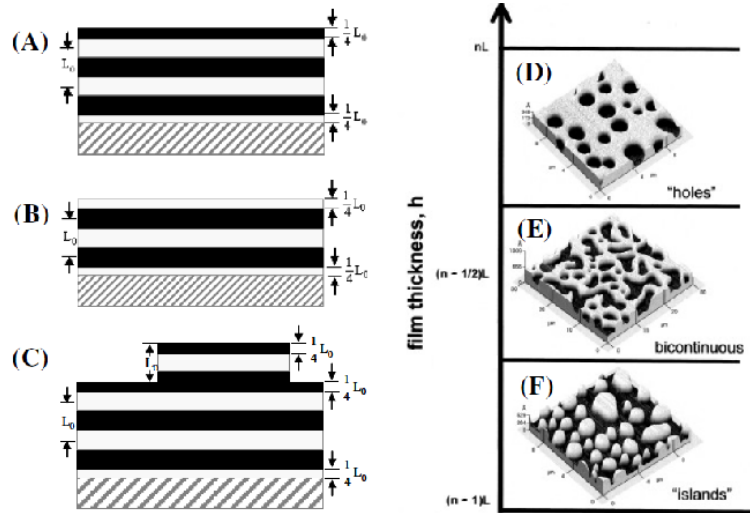


Figure 6.3: (a) Asymmetric wetting, (b) Symmetric wetting, (c) Formation of islands in the symmetric wetting case. The picture has been reproduced from reference [126]

asymmetric wetting $h = (n + 1/2)L$.

When the thickness of the DBC film before phase transition does not hold the right relation, the DBC in excess forms an incomplete layer. Therefore depending on the initial film thickness, a wide variety of surface morphology characterized by holes, islands or spinodal pattern are formed. [127, 128].

Under symmetric wetting conditions, said h the initial thickness of the film before organization:

- If $(n - 1/2)L < h < (n)L$ holes form on the surface of a film $(n)L$, with a depth of L (fig.6.3D)
- If $h(n + 1/2)$ we have the formation of a bicontinuous topography (serpentin or spinodal pattern) (fig.6.3E)
- If $(n - 1)L < h < (n - 1/2)L$ islands form on the surface with a L height over a base film $(n-1)L$ thick (fig.6.3F)

Under a-symmetric wetting conditions:

- If $nL < h < (n + 1/2)L$ holes form on the surface of a film $(n+1/2)L$, with a depth of L
- If hnL we have the formation of a bicontinuous topography (serpentin or spinodal pattern)
- If $(n - 1/2)L < h < nL$ islands form on the surface with a L height over a base film $(n-1/2)L$ thick

6.3 Samples preparation and characterization

The D-BC copolymer used in this work is a symmetric PS-b-PMMA, where PS stays for Polystyrene and PMMA stays for Polymethylmethacrylate. The molecular weight is $M_W = 89800g/mol$ ($M_{PS} = 49200g/mol$, $M_{PMMA} = 40600g/mol$), while polymerization degree is $N = 879$ ($N_{PS} = 473$, $N_{PMMA} = 406$). For this copolymer the bulk lamellar period L is approximately $38nm$.

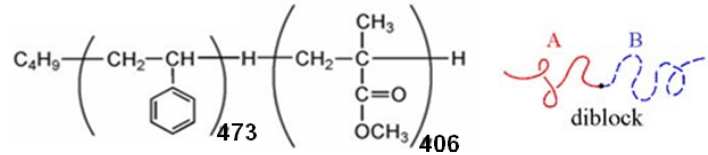


Figure 6.4: PS-b-PMMA diblock copolymer formula, the PS is indicated as the A block and The PMMA is indicated as the B block

PS-b-PMMA powder is dissolved in toluene, that is an organic solvent, and spin-coated on silicon wafers. The fast solvent evaporation occurring during spin-coating process causes the formation of an amorphous film in which polymer chains are randomly distributed. The film thickness has been varied by changing PS-b-PMMA concentration, maintaining the same spin-coating

parameters (acceleration= 2000rpm/s, speed=2000rpm, time= 30 s, exhaust volume= 50 μm). The percentages tested go from the 1% wt to the 5% wt and the thicknesses obtained are included into the range: 100-400 nm.

The thicknesses are measured by using ellipsometry and x-ray reflectivity. All the ellipsometric measurements have been performed at a wavelength $\lambda_e = 532$ nm and using an incidence angle varying in a small range around 60° , while for x-ray reflectivity the source wavelength used is $\lambda_X = 1.54$ Å and the incident angles are closed to zero.

In order to induce an alignment in the lamellar system, two techniques: the thermal and the solvent annealing have been used. In the thermal annealing samples are first brought up above the order-disorder transition temperature (T_{ODT}) and after are cooled down to room temperature. At high temperature ($T > T_{ODT}$), chains can move across the film and redistribute they-self to reach an equilibrium state. In the experiments, the annealing temperature is chosen to overcome glass transition temperature of both PS (100 °C) and PMMA (114°C), as reported in [128, 129]. The best experimental condition found is an annealing temperature of 180° for an annealing time of 72h. In the solvent annealing instead the films are exposed for several hours to the saturated vapors of a solvent. While in the previous method a higher chain mobility is induced by thermal agitation, in this case it is effect of the solvent absorption: moreover the presence of solvent molecules reduces the effect of repulsing interaction between blocks creating disorder. Solvents can be neutral (the film is uniformly swollen by solvent absorption) or selective (one block is swollen more than the other). Solvent selectivity is an important characteristic that can affect the resulting film morphology [130, 131]. The solvent chosen for experiments is the toluene (the same used for solution preparation), that is not selective. The sample are annealed in a chamber with an effective

volume of 30 cm^3 , the initial solvent volume is $10 \mu\text{L}$, and different annealing time have been tested. The chamber lid allows a very slow evaporation of the solvent, whose rate has been monitored during experiments. Beside ellipsometry and X-ray reflectivity, the annealed samples are characterized by optical microscopy and atomic force microscopy (AFM) in the tapping mode. A first check of the annealed sample is done by using optical microscopy; indeed the characteristic features present on the film surface (holes/islands) have a typical dimension of the order of few μm and the different thicknesses present in these samples can be seen as different discrete colors related to interference effects of the light reflected at the two interfaces. The AFM provides a topographical map of sample surface thus allowing a deeper understanding of surface morphologies.

6.4 Results for thermal annealing

In figure 6.5 optical and AFM images of a sample selection are reported.

Considering an asymmetric wetting, due to the preferential segregation of PMMA at the silicon substrate and to the lower PS surface energy [129], the initial film thickness h and a lamellar period not far from those measured in the bulk, the morphology presented are compatible with the explanation of section 6.2. In figure 6.5(a) the upper layer is almost complete, thus only small holes are present at the film surface ($h/L=2.9$); in figure 6.5(b) islands are forming a second incomplete layer and the situation is not far from a spinodal pattern in which the incomplete layer occupies almost half surface ($h/L=3.4$); the size of the holes in figure 6.5(c) is bigger than the one of the holes in figure 6.5(a) ($h/L=4.6$). Indeed the fraction of the film surface occupied by islands (or holes) in the ordered state is directly related to the initial film thickness

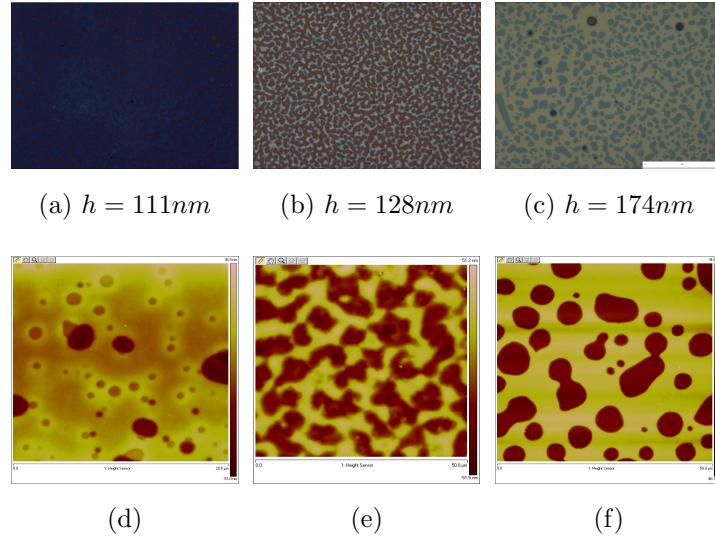


Figure 6.5: a) b) c) Optical microscopy pictures. Image size is $(300 \times 220) \mu m^2$; d) e) f) Corresponding AFM images. Image size is $(50 \times 50) \mu m^2$. The values h reported for each sample are the film thicknesses before annealing.

for mass conservation considerations [132]. Images (d), (e) and (f) of figure 6.5 are 2d projections of AFM topographical maps of the sample surface. The colored scale corresponds to the real height of the different layers present in the sample. In fig.6.6 three different sections of fig.6.5(f) are reported. Every hole in these images has the same depth, thus proving that the film is structured in an ordered lamellar system, moreover the depth value found (40 nm) is a direct measurement of the effective lamellar period L .

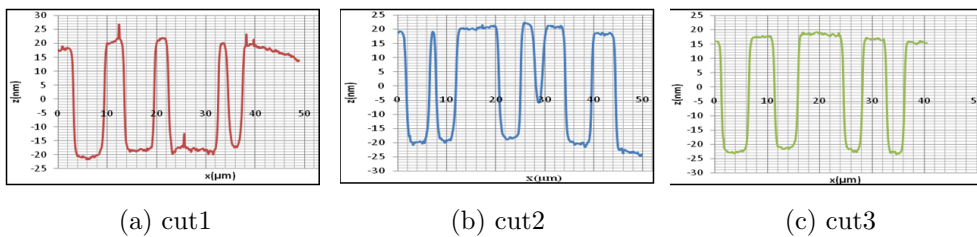


Figure 6.6: Three different cuts of the AFM measure shown in fig.6.5(f)

AFM measurements are also confirmed by x-ray reflectivity: the spectrum obtained for this sample (fig.6.7) does not exhibit the usual pattern observed

for amorphous film which was characterized by regular fringe spacing, it rather looks like a typical “beat” waveform as observed in reference [133] in the case of ordered lamellar systems. This “beat” phenomenon can be easily explained considering the superposition of the interference fringes due to the presence of two regions with different thickness. Keeping this in mind it is possible to estimate the lamellar period by fitting this spectrum with a “beat” waveform thus confirming the value measured using the AFM method ($L = 40$ nm).

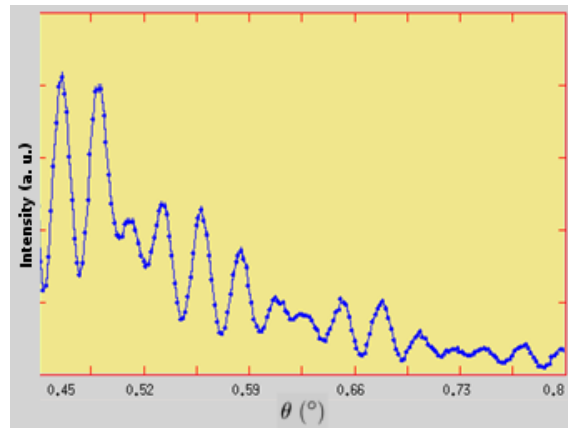


Figure 6.7: x-ray reflectivity spectrum, in function of the incident angle θ

6.5 Solvent annealing results

The optical images shown in fig.6.8 are related to different samples characterized by an initial film thickness of 150 nm when in the amorphous phase and all annealed by using the second experimental procedure described in section 6.3. The difference in between them is just the annealing time, namely the exposure time to the solvent which is indicated in the caption of each figure. It is evident that the shortest annealing times are not sufficient for DBC organization; indeed for $t = 2$ h any surface morphology it is observed, while for higher annealing time a weak surface morphology starts to appear in the

samples. The optimal equilibrium is reached for $t = 25$ h, where a neat surface morphology is evident.

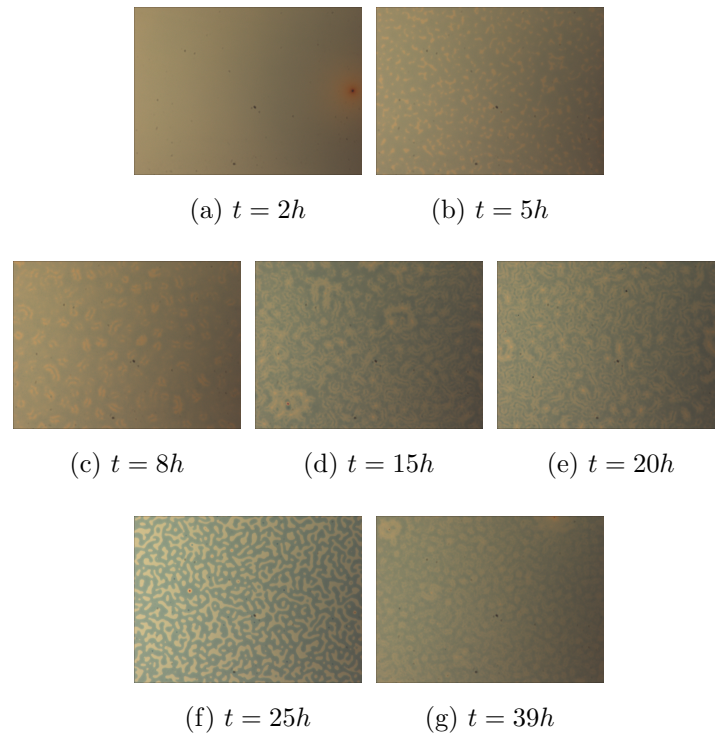


Figure 6.8: a) b) c) Optical microscopy pictures. Image size is $(300 \times 220) \mu m^2$; d) e) f) Corresponding AFM images. Image size is $(50 \times 50) \mu m^2$

X-ray reflectivity measurements show an increasing of surface roughness along with the annealing time, in fact a decreasing of fringe amplitude it is observed. Also AFM measurements demonstrate a higher roughness for samples realized by using solvent annealing if compared with samples realized by thermal annealing. In particular by evaluating a roughness value by means of a standard deviation we get a roughness value of 0.9 for the sample in fig.6.10 while the sample in fig. 6.5(f) presents a roughness value of just 0.45. On the other hand, on the spectrum related to the sample annealing for 25 hours, a single peak appears in the left part of the graph. This correspond to a second order Bragg peak ² meaning the film present a well organized

²the first order Bragg peak cannot be visualized because it is in the spectral region

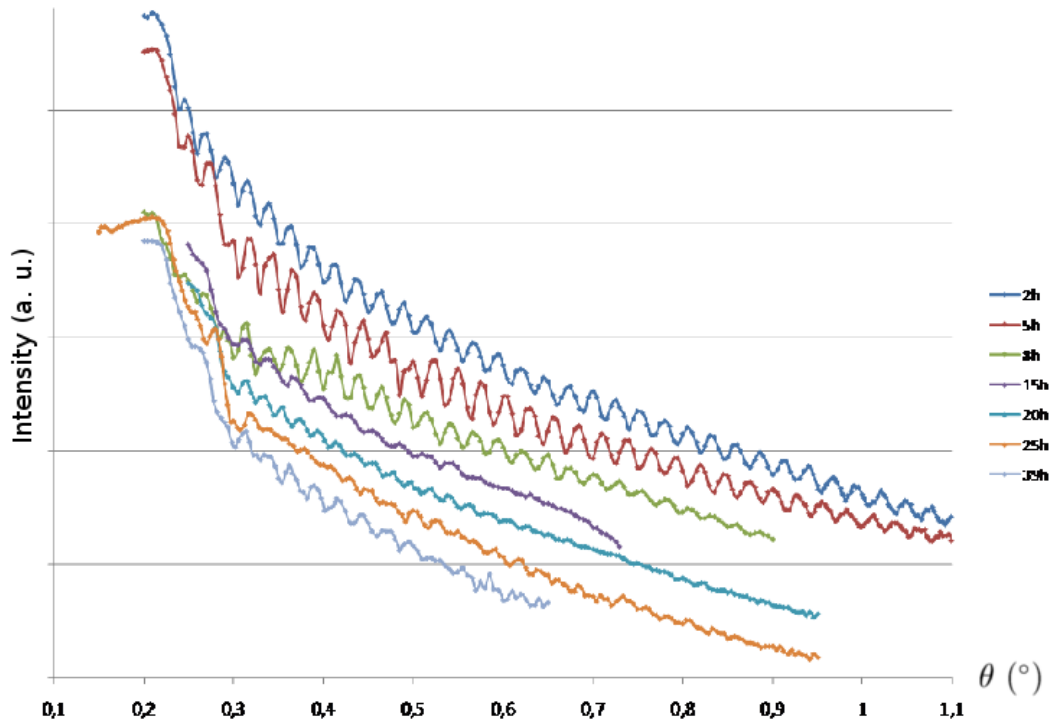


Figure 6.9: X-ray reflectivity spectra for the sample of fig.6.8

periodic structure whose period is comparable with the ones measured in the case of thermal annealed samples. In fig.6.10 are reported some measurements done for the sample annealed for 25 h. The spinodal texture visible in optical microscope image here is more evident.

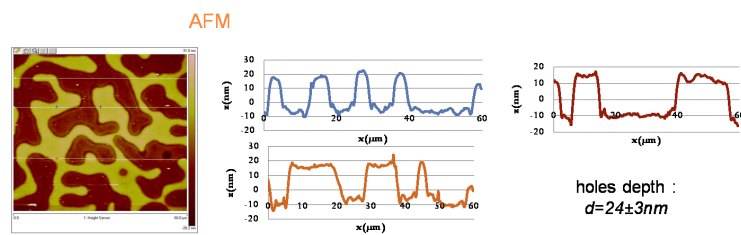


Figure 6.10: AFM measurements realized for the sample annealed for 25 h in toluene vapors

Also the depth of the spinodal structures present at the top surface of the dominated by total reflection

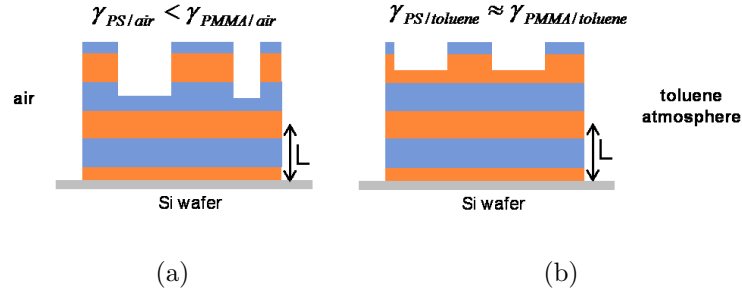


Figure 6.11: Illustration of the different microsegregation behavior of DBC organized by using thermal and solvent annealing

sample has been measured by AFM; the result obtained this time is quite different from that we expected. As shown in figure 6.10 it is around half time the expected lamellar period. The different DBC behavior in the two annealing methods can be explained considering the different environments in which DBC equilibrium is reached. In the solvent annealing the presence of toluene, that is a neutral solvent, changes the segregation conditions for the upper interface allowing both PS and PMMA to segregate at the free surface. As illustrated in fig.6.11: Indicating PMMA with the block A (orange layers in the figure), and PS with the block B (light-blue layers in the figure) the film structured by using thermal annealing are characterized by a sequence A-BB-AA-B (fig.6.11a), the incomplete layer formed with the polymer in excess is forced to be thick an entire lamellar period because of the preferential segregation of PS at the free surface resulting in the sequence A-BB-AA-BB-AA-B (fig.6.11b). In the solvent annealing case the complete layer is characterized by the sequence A-BB-AA-BB-A and the incomplete layer is composed by a single A-B (single molecule), because both A and B can segregate at the free surface.

The results obtained for both thermal and solvent annealing are consistent and both able to produce a well organized lamellar structure. In particular the

thermal annealing technique presents also a lower roughness in the produced structure however, due to the high temperature required by this technique it is hardly usable together with particular substrates or surface treatments. The presence of a surface morphology is an important evidence of lamellar organization but it is detrimental for optical applications, on the other hand obtaining flat substrates requires a fine control of the film thickness before annealing, that is very difficult considering the length scale involved. Another interesting possibility we explored is the development of a method for obtaining a perpendicular orientation of lamellæ to the substrate. As expected in the theory developed by Tsori [134], the production of substrates characterized by a suitable sinusoidal modulation can induce a perpendicular alignment. Some preliminary experiments have been performed on modulated substrates realized by photolithography, with a periodicity of 300 nm and an amplitude between 10-100 nm: while in flat surfaces produced by using the same photoresist evidences of parallel lamellæ alignments have been obtained, in the case of the modulated substrates, samples do not show any proof of organization remarking the strong influence the substrate has on the lamellæ organization.

Conclusions

In the present work we discussed two different experimental techniques: 2D POLICRYPS holographic curing and Di-block Copolymers self assembly, both able to realize 2D multicomponent structures but at different scales. These techniques are usable in a wide range of different applications, moreover being their common characteristic to present in the produced structures a complete phase separation between their constitutive components (NLC-NOA61, PS-PMMA) they are suitable candidate for any kind of confinements applications.

The first method discussed is based on the POLICRYPS gratings curing procedure which enable the realization of holographic gratings made of nematic liquid crystals and polymers and characterized by a strong phase separation. In this technique the grating is realized by impinging on the photosensitive material with a sinusoidal light pattern realized through the interference of two coherent laser beams in the UV range.

In order to extend this technique to 2D generic structures it has been used an SLM, namely a high resolution display, whose pixels can be separately controlled to apodize an impinging laser beam. The utilization of this highly technological and delicate device, forced us to firstly shift the POLICRYPS technique from UV radiation (that could eventually damage the device) to visible light. In the first section of the second chapter it is demonstrated that an alternative photosensitive syrup we proposed is suitable for the visible

POLICRYPS curing by characterizing a 1D Raman-Nath realized by using an interferometric set-up. The features of showed grating are in fact compatible with the one of a typical POLICRYPS grating. Once a good mixture to realize POLICRYPS structures in the visible has been found, we analyze some possible strategies to use the SLM for producing a generic curing light-pattern. In chapter 3 and 4 two approaches to produce a generic two dimensional light pattern with a SLM were considered. The first approach consist in the implementation of an Iterative Fourier Transform Algorithm (IFTA) for the calculation of a suitable phase function to be addressed on the SLM. While fascinating and widely usable for other applications this approach shows some issues when used for the realization of the high visibility patterns used for the realization of the micrometrical structures we are interested in. On the contrary the second considered method, the direct imaging, appeared to works fine for our purposes. In Chapter 4 we characterized some periodical structures realized with the POLICRYPS mixtures photosensitive in the visible range in order to demonstrate that they present in fact POLICRYPS features. Finally in Chapter 4 we chosen a fork-grating as an example of a a-periodic structure that can be realized with our 2D POLICRYPS technique, further demonstrating the wide range of technological applications this extension to the standard POLICRYPS technique can bring.

The second discussed method is based on self-assembling of a symmetric DBC confined in a thin film. The typical periodicities reached by using this technique are around of 40 nm. The two different annealing methods used to organize amorphous thin films show both clear evidences of a film organization with lamellae parallel to the silicon substrates. A comparative analysis based on AFM and X-ray microscopy document the appearing of the typical surface morphology due to thickness and lamellar period incommensurability. If of

one hand the appearing of hole and islands at the film surface is a strong proof of a parallel alignment, it is not desirable for optical applications. Controlling the thickness before annealing in order to reach flat annealed surface is a hard work considering that few nanometers of difference can totally change the surface morphology. A possible solution to overcome the problem is the induction of an alignment of lamellæ perpendicular to the the substrate. First attempts realized during the stage were promising: photoresist substrates with a sinusoidal modulation, have been used as neutralizing substrates. Even if perpendicular alignment has not been observed a different behavior of DBC on these modulated substrates if compared with flat substrates of the same photoresist indicated that we are following the right way. In the next future more experiments will be performed by changing amplitude and periodicity of the modulation in order to match the right parameters to induce a stable equilibrium of lamellæ aligned perpendicularly to the substrates.

Bibliography

- [1] R.L. Sutherland, L.V. Natarajan, V. P. Tondiglia, and T. J. Bunning. Bragg gratings in an acrylate polymer consisting of periodic polymer-dispersed liquid-crystal planes. *Chem. Mat.*, 5(10):1533–1538, 1993.
- [2] R. L. Sutherland, V. P. Tondiglia, L. V. Natarajan, T. J. Bunning, and W. W. Adams. Electrically switchable volume gratings in polymer-dispersed liquid crystals. *Appl. Phys. Lett.*, 64:1074–1076, 1994.
- [3] R. Caputo, A. V. Sukhov, C. Umeton, and R. F. Ushakov. Formation of a grating of submicron nematic layers by photopolymerization of nematic-containing mixtures. *Journal of Experimental and Theoretical Physics*, 91(6):1190–1197, 2000.
- [4] R. Caputo, A. V. Sukhov, C. Umeton, and R. F. Ushakov. Dynamics of mass transfer caused by the photoinduced spatially inhomogeneous modulation of mobility in a multicomponent medium. *Journal of Experimental and Theoretical Physics*, 92(1):28–36, 2001.
- [5] R. Caputo, L. De Sio, A. Veltri, C. Umeton, and A. V. Sukhov. Development of a new kind of switchable holographic grating made of liquid-crystal films separated by slices of polymeric material. *Opt. Lett.*, 29(11):1261–1263, 2004.

- [6] R. Caputo, A. Veltri, C. P. Umeton, and A. V. Sukhov. Characterization of the diffraction efficiency of new holographic gratings with a nematic film–polymer-slice sequence structure. *J. Opt. Soc. Am. B*, 21(11):1939–1947, 2004.
- [7] A. Marino, F. Vita, V. Tkachenko, R. Caputo, C. Umeton, A. Veltri, and G. Abbate. The european physical journal e: Soft matter biological physics. *Dynamical behaviour of holographic gratings with a nematic film Polymer slice sequence structure*, 15(1):47–52, Feb. 2004.
- [8] R. L. Sutherland, V. P. Tondiglia, L. V. Natarajan, S. Chandra, D. Tomlin, and T. J. Bunning. Switchable orthorhombic f photonic crystals formed by holographic polymerization-induced phase separation of liquid crystal. *Opt. Express*, 10(20):1074–1082, 2002.
- [9] S. P. Gorkhali, J. Qi, and G. P. Crawford. Electrically switchable mesoscale penrose quasicrystal structure. *Appl. Phys. Lett.*, 86, 2005.
- [10] S. P. Gorkhali, J. Qi, and G. P. Crawford. Switchable quasi-crystal structures with five-, seven-, and ninefold symmetries. *J. Opt. Soc. Am. B*, 23(1):149–158, 2006.
- [11] G. Zito, B. Piccirillo, E. Santamato, A. Marino, V. Tkachenko, and G. Abbate. Two-dimensional photonic quasicrystals by single beam computer-generated holography. *Opt. Express*, 16(8):5164–5170, 2008.
- [12] G. Zito, B. Piccirillo, E. Santamato, A. Marino, V. Tkachenko, and G. Abbate. Computer-generated holographic gratings in soft matter. *Molecular Crystals and Liquid Crystals*, 465:371–378, 2007.
- [13] Juntao Li, Yikun Liu, Xiangsheng Xie, Peiqing Zhang, Bing Liang, Li Yan1, Jianying Zhou, Gershon Kurizki, Daniel Jacobs, Kam Sing

- Wong, and Yongchun Zhong. Fabrication of photonic crystals with functional defects by one-step holographic lithography. *Opt. Express*, 16(17):12899, 2008.
- [14] N. Savage. Digital spatial light modulator. *Nature Photonics*, 3:170–172, 2009.
- [15] Iam-Choon Khoo. *Liquid Crystals:Physical Properties and Nonlinear Optical Phenomena*. John Wiley & Sons, New York, 1995.
- [16] P. G. de Gennes. *The physics of liquid crystals*, chapter 1. Clarendon Press, Oxford, 1995.
- [17] W.H. de Jeu G.Vertogen. *Termotropic Liquid Crystals, Fundamentals*. Springer-Verlag, Berlin, 1988.
- [18] F.Simoni. *Nonlinear Optical Properties of Liquid Crystals and Polymer Dispersed Liquid Crystals*, chapter 5. World Scientific, Singapore, 1997.
- [19] A.Yariv. *Optical Electronics*. Saunders College Publishing, California, 1991.
- [20] P. G. de Gennes. *The physics of liquid crystals*, chapter 4. Clarendon Press, Oxford, 1995.
- [21] W.H.de Jeu. *Physical Properties of Liquid Crystal Materials*. Gordon and Breach, New York, 1980.
- [22] P. G. de Gennes. *The physics of liquid crystals*, chapter 3. Clarendon Press, Oxford, 1995.
- [23] M. Born and E. Wolf. *Principles of Optics*, chapter XIV. Pergamon Press, NY, sixth edition, 1980.

- [24] A. Kumar and R. K. Gupta. *Fundamentals of Polymer Engineering, Revised and Expanded*, chapter I. CRC Press, 2003.
- [25] Y.J. Liu and X.W. Sun. Holographic polymer-dispersed liquid crystals: materials, formation, and applications. *Adv.in Optoelectronics*, 2008, 2008.
- [26] J.P. Fouer. *Photoinitiation, Photopolymerization and Photocuring: Fundamentals and Applications*, chapter 2. Hanser, München, 1995.
- [27] N.A. Vaz B.G. Wu J.W. Doane and S. Žumer. Field controlled scattering from nematic microdroplets. *Appl. Phys. Lett*, 48(269), 1986.
- [28] P.J.Drzaic. *Liquid Crystal Dispersions*. World Scientific, Singapore, 1995.
- [29] J.L.West. Phase separation of liquid crystals in polymers. *Mol.Cryst. Liq. Cryst.*, 157:427–441, 1988.
- [30] P.G. Drzaic. Polymer dispersed nematic liquid crystals for large area displays and light valves. *J.Appl.Phys.*, 60:2142, 1986.
- [31] G.W. Smith N.A. Vaz and G. Montgomery Jr. A light control film composed of liquid crystal droplets dispersed in a uv-curable polymer. *Mol.Cryst. Liq. Cryst.*, 146:1–15, 1987.
- [32] D. Gabor. A new microscopic principle. *Nature*, 161:777–778, 1948.
- [33] D. Gabor. Microscopy by reconstructed wavefronts. *Proc. Roy. Soc. A*, 197:454–487, 1949.
- [34] J.W. Goodman. *Introduction to Fourier Optics*. McGraw-Hill, New York, 1996.

- [35] E.G. Loewen and E. Popov. *Diffraction Gratings and Applications*, chapter 3. Marcel Dekker, Inc., New York-Basel, 1997.
- [36] M.G. Mohoram T.K. Gaylord. Thin and thick gratings: terminology clarification. *Appl. Opt.*, 20:3271.
- [37] W.R. Klein and B.D. Cook. Unified approach to ultrasonic light diffraction. *Sonics and Ultrasonics, IEEE*, 14(3):123, 1967.
- [38] L.Young and M.G. Mohoram. Criterion for bragg and raman-nath diffraction regimes. *Appl. Opt.*, 17(11):1757, 1978.
- [39] T.K. Gaylord and R.Magnusson. Analysis of multiwave diffraction gratings. *J.Opt.Soc.Am.*, 67(9):1165, 1977.
- [40] A. Lackner E. Ramos G. Smith N. Vaz J. Kohler Mangerum and C. Allison. Polymer dispersed liquid crystal film devices and method of forming the same. *US Patent 4,938,568*, 1990.
- [41] Nuno A. Vaz; George W. Smith; G. Paul Montgomery Jr. Polymer dispersed liquid crystal film devices. *US Patent 5,096,282*, 1992.
- [42] J.W. Doane Z.Yaniv R. L. Sutherland. Optical limits, switches and filters based on polymer dispersed liquid crystal. In *Liquid Crystal Chemistry, Physics and a Applications*, volume 1080 of *Proc.Soc.Photo-Opt.Instrum.*, 1989.
- [43] J.D. Margerum E. Ramos K.-C. Lim A.M. Lackner. *Proc. SOC. Photo-Opt. Instrum. Eng*, 1080(53), 1989.
- [44] V.P. Tondiglia L.V. Natarajan T.J. Bunning R.L. Sutherland and W.W. Adams. Volume holographic image storage and electro-optical readout in a polymerdispersed liquid crystal film. *Opt.Lett.*, 20(1325), 1995.

- [45] V.P. Tondiglia L.V. Natarajan T.J. Bunning W.W.Adams R.L. Sutherland. Electro-optical switching characteristics of volume holograms in polymer dispersed liquid crystals. *J. Nonlinear Opt. Phys. Materials*, 5(90), 1996.
- [46] R.L. Sutherland. Polarization and switching properties of holographic polymer-dispersed liquid-crystal gratings i. theoretical model. *J. Opt. Soc. Am. B*, (12):2995, 2002.
- [47] L.V. Natarajan, V.P. Tondiglia, S. Chandra, C.K. Shepherd, D.M. Brandelik, S.A. Siwecki, R.L. Sutherland, and T. J. Bunning. Polarization and switching properties of holographic polymer-dispersed liquid-crystal gratings ii. experimental investigations, 2002. *J. Opt. Soc. Am. B*, 19(12):3004.
- [48] J. Colegrove G. Hu T. Fiske A. Lewis J. Gunther L. Silverstein C. Bowley G.Crawford L. Chien J. Kelly H. Yuan. Hpdlc color reflective displays. *Proc. SPIE*, 3690(196), 1999.
- [49] G.P. Crawford. Electrically switchable bragg gratings. 14(4):54. *Optics and Photonics News*, 14(4):54, 2003.
- [50] R. L. Sutherland, V. P. Tondiglia, L. V. Natarajan, and S. Chandra. Switchable orthorhombic f photonic crystals formed by holographic polymerization-induced phase separation of liquid crystal. *Opt. Express*, 10(20):1074, 2002.
- [51] V. P. Tondiglia, L. V. Natarajan, R. L. Sutherland, D. Tomlin, and T. J. Bunning. Holographic formation of electro-optical polymer-liquid crystal photonic crystals. *Adv.Mat.*, 14(3):187–191, 2002.

- [52] Y.J. Liu and X.W. Sun. Electrically tunable two-dimensional holographic photonic crystal fabricated by a single diffractive element. *Appl. Phys. Lett*, 89:171101–171103, 2006.
- [53] V.P. Tondiglia L.V. Natarajan R.L. Sutherland P. Lloyd T.J. Bunning R.A. Vaia R.Jakubiak. *Adv.Mat.*, 17:2807, 2005.
- [54] D.E. Lucchetta, L. Criante, O. Francescangeli, and F. Simoni. Wavelength flipping in laser emission driven by a switchable holographic grating. *Appl. Phys. Lett*, 84:837–839, 2004.
- [55] D.E. Lucchetta, L. Criante, O. Francescangeli, and F. Simoni. Light amplification by dye-doped holographic polymer dispersed liquid crystals. *Appl. Phys. Lett*, 84:4893–4895, 2004.
- [56] W.D. Kirkey F.Chen A.N. Cartwright P.N. Prasad T.J. Bunning V.K.S. Hasiao. Organic solvent vapor detection using holographic photopolymer reflection gratings. *Adv.Mat.*, pages 2211–2214, 2005.
- [57] A. Veltri, R. Caputo, C. Umeton, and A. V. Sukhov. Model for the photoinduced formation of diffraction gratings in liquid-crystalline composite materials. *Appl. Phys. Lett.*, 84:3492–3494, Jan. 2004.
- [58] T. Karasawa and Y. Taketomi. Effects of material systems on the polarization behavior of holographic polymer dispersed liquid crystal gratings. *Jpn. J. Appl. Phys.*, 36:6388–6392, 1997.
- [59] J. Qi, M. De Sarkar, G.T. Warren, and G.P. Crawford. and. In situ shrinkage measurements of holographic polymer dispersed liquid crystals. *J. Appl. Phys.*, 91:4795, 2002.

- [60] M.S. Park, Y.H. Cho, B.K. kim, and J.S. Jang. Fabrication of reflective holographic gratings with polyurethane acrylate. *Curr. Appl. Phys.*, 2:249, 2002.
- [61] R.A. Ramsey and S.C. Charma. Holographically recorded reverse-mode transmission gratings in polyme dispesed liquid crystal cells. *Appl. Phys. B*, 93:481–489, 2008.
- [62] V.P. Tondiglia, R.L. Sutherland, L. V. Natarajan, P.E. Lloyd, and T. J. Bunning. Droplet deformation and alignment for high- efficiency polarization-dependent holographic polymer-dispersed liquid-crystal reflection gratings. *Opt. Lett.*, 33(16):1890–1892, 2008.
- [63] D.E. Lucchetta, R. Karapinar, A. Manni, and F. Simoni. Phase only modulation by nanosized polymer-dispersed liquid crystals. *J. Appl. Phys.*, 91:6060, 2002.
- [64] D. E. Lucchetta, L. Criante, and F. Simoni. Optical characterization of polymer dispersed liquid crystals for holographic recording. *J. Appl. Phys.*, 93:9669–9674, 2003.
- [65] R. Caputo, A. V. Sukhov, C. Umeton, and R. F. Ushakov. Formation of a grating of submicron nematic layers by photopolymerization of nematic-containing mixtures. *J.of Exp. and Theor. Phys.*, 91(6):1190–1197, 2000.
- [66] R. Caputo, L. De Sio, A. Veltri, C. Umeton, and A. V. Sukhov. Policryps switchable holographic grating: A promising grating electro-optical pixel for high resolution display application. *J. Display Technol.*, 2(1):38, 2006.

- [67] L. De Sio, N. Tabiryan, R. Caputo, A. Veltri, and C. P. Umeton. Polycryps as structures as switchable optical phase modulators. *Opt. Express*, 16(11):7619–7624, 2008.
- [68] R. Caputo, A. De Luca, L. De Sio, L. Pezzi, G Strangi1, C.P. Umeton, A. Veltri, R. Asquini, A. dAlessandro, D Donisi, R. Beccherelli, A.V. Sukhovand N V Tabiryan5, and N.V. Tabiryan. Polycryps: a liquid crystal composed nano/microstructure with a wide range of optical and electro-optical applications. *J. of Opt. A*, 11:024017, 2009.
- [69] L. De Sio and C. Umeton. Dual-mode control of light by 2d periodic structures realized in liquid-crystalline composite materials. *to be published in Optics Letters*, 2010.
- [70] R. Caputo, A.V. Sukhov, N.V. Tabirian, C. Umeton, and R.F. Ushakov. Mass transfer processes induced by inhomogeneous photo-polymerisation in a multicomponent medium. *Chemical Physics*, 271:323–335, 2001.
- [71] T. Kelly and J. Munch. Phase-aberration correction with dual liquid crystal spatial light modulator. *Appl. Opt.*, 37(22):5184–5189, 1998.
- [72] N. Hashimoto, S. Morakawa, and K. Kitamura. Real-time holography using the high-resolution lctv-slm. *Proc. SPIE Pratical Holography V*, S.A. Benton ed., 1461:291–302, 1991.
- [73] D. G. Grier. A revolution in optical manipulation. *Nature*, 424:810–816, 2003.
- [74] C.E. Hoyle, T.Y. Lee, and T. Roper. Thiol-enes: Chemistry of the past with promise for the future. *J. Pol. Sci.: part A: Pol. Chem.*, 42:5301–5338, 2004.

- [75] M.J. kade, D.J. Burke, and C.J. Hawker. The power of thiol-ene chemistry. *J. Pol. Sci.: part A: Pol. Chem.*, 48:743–750, 2009.
- [76] S.A. Khan. Effect od shears on the gelation of uv curable polymers. *J. Rheol.*, 36(4):573–587, 1992.
- [77] X. Gong, W. Wen, and P. Scheng. Microfluidic fabrication of porous polymer microspheres: Dual reactions. *Langmuir*, 25(4):7072–7077, 2009.
- [78] T. J. Bunning, L. V. Natarajan, V.P. Tondiglia, G. Dougherty, and R.L. Sutherland. Morphology of anisotropic polymer-dispersed liquid crystals and the effect of monomer functionality. *J. Pol. Sci.: part A: Pol. Chem.*, 35:2825–2833, 1997.
- [79] T. J. White, L. V. Natarajan, V. P. Tondiglia, P. F. Lloyd, T. J. Bunning, and C. A. Guyman. Monomer functionality effects in the formation of thiol-ene holographic polymer dispersed liquid crystals. *Macromolecules*, 40(4):1121–1127, 2007.
- [80] T. J. White, W. B. Liechty, L. V. Natarajan, V. P. Tondiglia, T. J. Bunning, and C. A. Guyman. The influence of n-vinyl-2-pyrrolidone in polymerization of holographic polymer dispersed liquid crystals. *Polymer*, 47:2289–2298, 2006.
- [81] S. H. Lin, Y-N. Hsiao, and K.Y. Hsu. Preparation and characterization of irgacure 784 doped photopolymers for holographic recording. *J. Opt. A: Pure Appl. Opt.*, 11:024012–024020, 2009.
- [82] L. V. Natarajan, D. P. Brown, J. M. Wofford, V.P. Tondiglia, R. L. Sutherland, P. F. Lloyd, and T. J. Bunning. Holographic polymer dis-

persed liquid crystal reflection gratings formed by visible light initiated thiol-ene polymerization. *Polymer*, 47:4411–4420, 2006.

- [83] J.W. Goodman. *Introduction to Fourier Optics*, chapter 5. McGraw-Hill, New York, second edition, 1996.
- [84] J. W. Goodman. *Introduction to Fourier Optics*, chapter 3. McGraw-Hill, New York, second edition, 1996.
- [85] M. Born and E. Wolf. *Principles of Optics*, chapter 8. Pergamon Press, sixth edition, 1980.
- [86] V.A. Soifer, V. Kotlyar, and L. Doskolovich. *Iterative Methods for Diffractive Optical Elements Computation*. Taylor & Francis Routledge, 1997.
- [87] R. W. Gerberch and W. O. Saxton. A practical algorithm for the determination of phase from image and diffraction plane pictures. *Optik*, 35(2):237–246, 1972.
- [88] J.R. Fineup. Reconstruction of an object from the modulus of its fourier transform. *Opt. Lett.*, 3(1):27–29, 1978.
- [89] H. Kim and B. Lee. Optical nonmonotonic convergence of the iterative fourier-tranform algorithm. *Opt. Lett.*, 30(3):296–298, 2005.
- [90] M. Guizar-Sicairos and J.R. Fineup. Phase retrieval with fourier-weighted projections. *J. Opt. Soc. Am. A*, 25(3):701–706, 2008.
- [91] M. Pasienski and B. DeMarco. A high-accuracy algorithm for designing arbitrary holographic atom traps. *Opt. Express*, 16(3):2176–2190, 2008.

- [92] F. Wyrowski and O. Bryngdahl. Iterative fourier transform algorithm applied to computer holography. *J. Opt. Soc. Am. A*, 5(7):1058–1065, 1988.
- [93] P. Senthilkumaran, F. Wyrowski, and H. Shimmel. Vortex stagnation problem in iterative fourier transform algorithms. *Opt. Las. Eng.*, 43:43–56, 2005.
- [94] H. Aagedal, M. Schmid, T. Beth, S. Tiewes, and F. Wyrowski. Theory of speckles in diffractive optics and its application to beam shaping. *J. Mod. Opt.*, 43:1409–1421, 1996.
- [95] V. Arrizòn and M. Testorf. Efficiency limit of spatially quantized fourier array illuminators. *Opt. Lett.*, 22(4):197–199, 1997.
- [96] F. Wyrowski. Upper bound of the diffraction efficiency of diffractive phase elements. *Opt. Lett.*, 16(24):1915–1917, 1991.
- [97] J.W. Goodman and A.M. Silvestri. Some effects of fourier-domain phase quantization. *IBM J. Res. Devel*, 14(5):478, 1970.
- [98] V. Arrizòn, E. Carreòn, and M. Testorf. Implementation of fourier array illuminators using pixelated slm: efficiency limitations. *Opt. Comm.*, 160:207–213, 1999.
- [99] D. Palima and V.R. Daria. Effect of spurious diffraction orders in arbitrary multifoci patterns produced via phase-only holograms. *Appl. Opt.*, 45(26):6689–6693, 2006.
- [100] I. Moreno, J. Campos, C. Gorecki, and M.J. Yzuek. Effect of amplitude and phase mismatching errors in the generation of a kinoform for pattern recognition. *Jpn. J. Appl. Phys.*, 34:6423–6432, 1995.

- [101] D. Palima and V.R. Daria. Holographic projection of arbitrary light patterns with a suppressed zero-order beam. *Appl. Opt.*, 46(20):4197–4201, 2007.
- [102] E. O. Brigham. *Fast Fourier Transform*. Prentice-Hall, Englewood Cliffs, NJ, 1974.
- [103] J.A. Davis, K.O. Valadéz, and D. M. Cottrell. Encoding amplitude and phase information onto a binary phase-only spatial light modulator. *Appl. Opt.*, 42(11):2003–2008, 2003.
- [104] J. A. Davis, S. W. Flowers, D. M. Cottrell, and R.A. Lilly. Smoothing of the edge-enhanced impulse response from binary phase-only filters using random binary patterns. *Applied Optics*, 28:2987–2988, 1989.
- [105] K. T. Gahagan and Jr. G. A. Swartzlander. "optical vortex trapping of particles". *Opt. Lett.*, 21(11):827–829, 1996.
- [106] K. T. Gahagan and Jr. G. A. Swartzlander. Trapping of low-index microparticles in an optical vortex. *J. Opt. Soc. Am. B*, 15(2):524–534, 1998.
- [107] A. Kumar, P. Vaity, Y. Krishna, and R.P. Singh. "engineering the size of dark core of an optical vortex". *Opt. and Las. in Eng.*, 48:276–281, 2010.
- [108] A.V. Carpentier, H. Michinel, and J.R. Salgueiro. "making optical vortices with computer-generated holograms". *Am. J. Phys.*, 76(10):916–921, 2008.
- [109] I.W. Hamley. *The physics of block copolymers*. Oxford University Press, Oxford, 1998.

- [110] I.W. Hamley. *Developments in block copolymer science and technology*. John Wiley & Sons, Chichester, 2004.
- [111] M. Lazzari, G. Liu, and S. Lecommandoux. *Block copolymer in nanoscience*. Wiley-VCH, 2006.
- [112] L. Leibler. Theory of micro-phase separation in block copolymers. *Macromolecules*, 13:1602–1617, 1980.
- [113] F. S. Bates. Polymer-polymer phase behavior. *Science*, 251(4996):898–905, 1991.
- [114] G.H. Fredrickson and F.S. Bates. Dynamics of block copolymers : theory and experiments. *Ann. Rev. Mater. Sci.*, 26:501–550, 1996.
- [115] H.-A. Klok and S. Lecommandoux. Supramolecular materials via block copolymer self-assembling. *Adv.Mat.*, 13(16):1217–1229, 2001.
- [116] A. Jo, W. Joo, W.-H. Jin, H. Nam, and J.K. Kim. Ultrahigh-density phase-change data storage without the use of heating. *Nature Nanotech.*, 4:727–731, 2009.
- [117] M. Park, C. Harrison, P.M. Chaikin, R.A. Register, and D.H. Adamson. Block copolymer lithography: Periodic arrays of 10^{11} holes in 1 square centimeter. *Science*, 276(5317):1401–1404, 1997.
- [118] Y. Lin, A. Böker, J. He, K. Sill, H. Xiang, C. Abetz, X. Li, J. Wang, T. Emrick, S. Long, Q. Wang, A. Balazs, and T.P. Russell. Self-directed self-assembly of nanoparticle/copolymer mixtures. *Nature*, 434:55–59, 2005.

- [119] Z.-R. Chen, J. A. Kornfield, S.D. Smith, J.T. Grothaus, and M. M. Sattkowsky. Pathways to macroscale order in nanostructured block copolymers. *Science*, 277(5330):1248–1253, 1997.
- [120] I.W. Hamley. Structure and flow behaviour of block copolymers. *J.Phys.: Cond.Matter.*, 13(33), 2001.
- [121] K. Amundson, E. Helfand, X. Quan, S.D. Hudson, and S.D. Smith. Alignment of lamellar block copolymer microstructure in an electric field. 2. mechanisms of alignment. *Macromolecules*, 27(22):6559–6570, 1994.
- [122] I.W. Hamley. Ordering in thin films of block copolymers: Fundamentals to potential applications. *Progr.Polym.Sci.*, 34(11):1161–1210, 2009.
- [123] J.-Y. Wang, S. Park, and T.P. Russell. *Polymer thin films*, chapter 1. World Scientific Publishing & Co., 2010.
- [124] G.H. Fredrickson. Surface ordering phenomena in block copolymer melts. *Macromolecules*, 20(10):2535–2542, 1987.
- [125] S. H. Anastasiadis, T. P.Russell, S. K. Satija, and C. F.Majkrzak. Neutron reflectivity studies of the surface-induced ordering of diblock copolymer films. *Phys. Rev. Lett.*, 62(16):1852–1855, 1989.
- [126] P.F. Green and R. Limary. Block copolymer thin films: pattern formation and phase behavior. *Adv. Colloid Int. Sci.*, 94:53–81, 2001.
- [127] A.P. Smith, A. Sehgal, J.F. Douglas, A. Karim, and E.J. Amis. Combinatorial mapping of surface energy effects on diblock copolymer thin film ordering. *Macromol. Rapid Commun.*, 24:131–135, 2003.
- [128] A.P. Smith, J.F. Douglas, J. Carson Meredith, E.J. Amis, and A. Karim. High-throughput characterization of pattern formation in symmetric di-

- block copolymer films. *J. Pol. Sci.: part B: Pol. Phys.*, 39:2141–2158, 2001.
- [129] T. P. Russell, G. Coulon, V. R. Deline, and D. C. Miller. Characteristics of the surface-induced orientation for symmetric diblock ps/pmma copolymers. *Macromolecules*, 22:4600–4606, 1989.
- [130] J. Peng, Y. Xuan, H. Wang, Y. Yang, B. Li, and Y. Han. Solvent-induced microphase separation in diblock copolymer thin films with reversibly switchable morphology. *J. Chem. Phys.*, 120(23):11163–11170, 2004.
- [131] J. Peng, D.H. Kim, W. Knoll, Y. Xuan, B. Li, and Y. Huan. Morphologies in solvent-annealed thin films of symmetric diblock copolymer. *J. Chem. Phys.*, 125(064702), 2006.
- [132] B. Collin, D. Chatenay, G. Coulon, D. Ausserre, and Y. Gallot. Ordering of copolymer thin films as revealed by atomic force microscopy. *Macromolecules*, 25(5):1621–1622, 1992.
- [133] G. Vignaud, A. Gibaud, G. Grubel, S. Joly, J.F. Legrand, and Y. Gallot. Ordering of diblock ps-pbma thin films: An x-ray reflectivity study. *Physica B*, 248:250–257, 1998.
- [134] Y. Tsori, E. Sivaniah, Andelman, and T. Hashimoto. Orientational transitions in symmetric diblock copolymers on rough surfaces. *Macromolecules*, 38:7193–7196, 2005.